1 **TITLE**

# 2 Lysine63-linked ubiquitin chains earmark GPCRs for BBSome-
# 3 mediated removal from cilia

4 **AUTHORS:** Swapnil Rohidas Shinde, Andrew R. Nager# and Maxence V. Nachury*

5 **AFFILIATION:**

6 Department of Ophthalmology, University of California San Francisco, CA 94143, USA

7

8 * Correspondence: maxence.nachury@ucsf.edu

9 # Current address: Cancer Immunology Discovery, Pfizer Inc., San Diego, CA, 92121, USA

**ABSTRACT (158 words)**

Regulated trafficking of G-protein coupled receptors (GPCRs) controls cilium-based signaling pathways. β-arrestin, a molecular sensor of activated GPCRs, and the BBSome, a complex of Bardet-Biedl Syndrome (BBS) proteins, are required for the signal-dependent exit of ciliary GPCRs but the functional interplay between β-arrestin and the BBSome remains elusive. Here we find that, upon activation, ciliary GPCRs become tagged with K63-linked ubiquitin (K63Ub) chains in a β-arrestin-dependent manner prior to BBSome-mediated exit. Removal of ubiquitin acceptor residues from the somatostatin receptor 3 (SSTR3) and from the orphan GPCR GPR161 demonstrates that ubiquitination of ciliary GPCRs is required for their regulated exit from cilia. Furthermore, targeting a K63Ub-specific deubiquitinase to cilia blocks the exit of GPR161, SSTR3 and Smoothened (SMO) from cilia. Finally, ubiquitinated proteins accumulate in cilia of mammalian photoreceptors and *Chlamydomonas* cells when BBSome function is compromised. We conclude that K63Ub chains mark GPCRs and other unwanted ciliary proteins for recognition by the ciliary exit machinery.

## INTRODUCTION

The regulated trafficking of signaling receptors in and out of cilia is a central regulatory mechanism of many cilia-based signaling pathways (Nachury and Mick, 2019; Anvarian et al., 2019; Mykytyn and Askwith, 2017; Gigante and Caspary, 2020). For example, upon activation of the Hedgehog signaling pathway, the Hedgehog receptor Patched 1 and the G protein-coupled receptor (GPCR) GPR161 disappear from cilia while GPCR Smoothened (SMO) accumulates in cilia (Rohatgi et al., 2007; Corbit et al., 2005; Mukhopadhyay et al., 2013). In all three cases, regulated exit from cilia plays a major role in the on-demand redistribution of signaling molecules (Nachury and Mick, 2019). Signal-dependent exit is likely to be a general characteristic of ciliary GPCRs as the Somatostatin Receptor 3 (SSTR3), the Dopamine Receptor 1 (D1R), the Melanocortin concentrating hormone receptor 1 (MCHR1) and the neuropeptide receptor 2 (NPY2R) all disappear from cilia upon exposure to agonist (Domire et al., 2011; Loktev and Jackson, 2013; Nager et al., 2017; Green et al., 2015). A major question is how GPCRs are selected for removal from cilia in an activity-dependent manner.

The major trafficking entities mediating signal-dependent exit from cilia are the BBSome and β-arrestin 2. The BBSome is an evolutionarily conserved complex of eight Bardet-Biedl Syndrome (BBS) proteins that directly recognizes intracellular determinants in GPCRs and ferries them out of cilia (Nachury, 2018; Wingfield et al., 2018). The BBSome associates with the intraflagellar transport (IFT) machinery and has been proposed to act as adaptor between the motor-driven intraflagellar transport trains and the membrane proteins that are to be removed from cilia. Because the BBSome is not known to have the ability to discriminate active from inactive GPCRs, there must exist another layer of regulation that commits activated GPCRs for exit. β-arrestin 2 is a well-established molecular sensor of the activation state of GPCRs that is required for the signal-dependent exit of GPR161 and SSTR3 (Pal et al., 2016; Green et al., 2015; Nager et al., 2017). No association of β-arrestin 2 with ciliary trafficking complexes has been reported to date and it remains unclear how β-arrestin 2 relays information regarding the state of activation of ciliary GPCRs to the ciliary exit machinery.

53 An emerging player in ciliary exit is ubiquitination (Shearer and Saunders, 2016). Ubiquitin (Ub),
54 a 76-amino acid polypeptide, becomes conjugated to acceptor lysine residues on substrate
55 proteins by ubiquitin ligases and tags substrates for degradation or other regulatory fates (Yau
56 and Rape, 2016; Swatek and Komander, 2016). A role for ubiquitin in promoting ciliary exit is
57 suggested by multiple lines of evidence. First, interfering with Patched1 ubiquitination blocks its
58 signal-dependent exit from cilia (Kim et al., 2015; Yue et al., 2014). Second, fusing ubiquitin to
59 PKD-2, the olfactory receptor ODR-10 or the TRP channel OSM-9 at their cytoplasmic end
60 results in the disappearance of these proteins from cilia (Hu et al., 2007; Xu et al., 2015). The
61 accumulation of these ubiquitin fusions inside cilia when BBSome function is compromised
62 suggests that the BBSome might sort ubiquitinated signaling receptors out of cilia, in line with a
63 reported association of BBSome with ubiquitinated proteins in trypanosomes (Langousis et al.,
64 2016). Interestingly, TRIM32 is a ubiquitin ligase mutated in BBS patients (Chiang et al., 2006).
65 Third, the ubiquitin ligase Cbl is recruited to cilia upon activation of the ciliary tyrosine kinase
66 receptor PDGFRαα and Cbl is required for termination of PDGFRαα signaling (Schmid et al.,
67 2018). Last, a dramatic rise in ubiquitination of the ciliary proteome is observed when
68 *Chlamydomonas* cilia disassemble (Huang et al., 2009). In particular, α-tubulin becomes
69 ubiquitinated on K304 upon cilia disassembly and expression of α-tubulin[K304R] slows down
70 cilia disassembly (Wang et al., 2019).
71 After conjugation onto substrates, ubiquitin itself often serves as a substrate for ubiquitination.
72 The resulting ubiquitin chains are characterized by the acceptor lysine residue on ubiquitin with
73 lysine 48-linked Ub (UbK48) chains targeting soluble proteins for proteasomal degradation while
74 lysine 63-linked Ub (UbK63) chains assembled onto membrane proteins constitute the major
75 driver for sorting from the limiting membrane of late endosomes into intralumenal vesicles and
76 ultimately lysosomal degradation (Piper et al., 2014; Yau and Rape, 2016; Swatek and
77 Komander, 2016). Intriguingly, in shortening *Chlamydomonas* cilia K63Ub linkages predominate
78 at least 5-fold over K48 linkages and only K63Ub linkages are detected on α-tubulin. A role for
79 K63Ub chains in ciliary trafficking remains to be determined.

80 Together, these data led us to investigate the interplay between ubiquitination, β-arrestin 2 and
81 the ciliary exit machinery. Using a combination of cellular imaging, biochemical studies and
82 cilia-specific manipulations, we find that β-arrestin 2 directs the activation-dependent addition of
83 K63-linked ubiquitin chains onto ciliary GPCRs that are then selected by the BBSome for
84 removal from cilia.

## RESULTS

### Signal-dependent ubiquitination of ciliary GPCRs is required for their regulated exit from cilia

As a first step in investigating the interplay between ubiquitination and the ciliary exit machinery, we sought to determine whether activation of ciliary GPCRs leads to their ubiquitination inside cilia prior to retrieval into the cell. We blocked BBSome-dependent exit by deleting its cognate GTPase ARL6/BBS3 in mouse inner medulla collecting duct (IMCD3) cells. IMCD3 cells represent a validated cell culture system to study ciliary trafficking and the IMCD3 *Arl6*$^{-/-}$ line has been previously characterized (Liew et al., 2014; Ye et al., 2018). As in previous studies (Ye et al., 2018; Nager et al., 2017), all GPCRs were expressed at near-endogenous levels by driving expression with extremely weak promoters. The fluorescent protein mNeonGreen (NG) fused to the cytoplasm-facing C-terminus of GPCRs allowed direct visualization. A biotinylation Acceptor Peptide (AP) fused to the extracellular N-terminus biotinylated by an ER-localized biotin ligase (BirA-ER) enabled pulse labeling of surface-exposed molecules and denaturing purifications. When SSTR3 was expressed in *Arl6*$^{-/-}$ IMCD3 cells, addition of its agonist somatostatin (sst) led to a drastic increase in the ciliary levels of ubiquitin observed upon immunostaining with the well-characterized FK2 (**Figure 1A-B)** and FK1 (**Figure S1A-B**) monoclonal antibodies (Fujimuro et al., 1994; Emmerich and Cohen, 2015; Haglund et al., 2003). All further experiments were conducted with the FK2 antibody. *Arl6*$^{-/-}$ cells accumulated Ub signals inside cilia in the absence of SSTR3 expression (**Figure 1A-B**), demonstrating that some endogenous proteins become ubiquitinated inside the cilia of *Arl6*$^{-/-}$ IMCD3 cells. No ubiquitin signal was detected inside cilia when BBSome function was intact (**Figure 1A-B and S1A-D**), indicating that the BBSome efficiently removes ubiquitinated proteins from cilia. Because the sst-dependent increase in ciliary ubiquitin signal depends upon SSTR3 expression (**Figure 1A-B**), these results suggest that either SSTR3 itself or a downstream effector of SSTR3 become ubiquitinated inside cilia upon activation.

111 To determine whether SSTR3 becomes ubiquitinated in response to sst, we biochemically
112 isolated $^{AP}$SSTR3$^{NG}$ under denaturing conditions via the biotinylated AP tag and probed for
113 ubiquitin via an HA tag on transfected HA-Ub. As typical for a glycosylated protein, SSTR3
114 migrated as a broad band centered around 100 kDa (**Figure 1C**). The amount of SSTR3
115 recovered did not change appreciably between WT and *Arl6*$^{-/-}$ cells or upon stimulation with sst
116 (**Figure 1C**). Remarkably, while only very faint Ub signals were detected associated with SSTR3
117 in WT cells, a Ub smear extending from 100 kDa upward was detected in the SSTR3 pull-downs
118 from *Arl6*$^{-/-}$ cells. Furthermore, stimulation with sst resulted in a modest but reproducible
119 increase in SSTR3 ubiquitination in *Arl6*$^{-/-}$ cells (**Figure 1D**). We conclude that the
120 BBSome/ARL6 system is required for the degradation of ubiquitinated SSTR3 and that SSTR3
121 becomes ubiquitinated in response to stimulation with sst.

122 We next sought to test whether signaling receptors endogenous to IMCD3 cells are ubiquitinated
123 inside cilia in an activity-dependent manner. One signaling pathway that is natively expressed in
124 IMCD3 cells is the Hedgehog pathway. Prior experiments have detected normal trafficking
125 dynamics of SMO and GPR161 in IMCD3 cells (Ye et al., 2018; Mukhopadhyay et al., 2013)
126 and **Figure 4D**). As GPR161 and SMO both accumulate in cilia of *Arl6*$^{-/-}$ cells without Hh
127 pathway stimulation (Liew et al., 2014; Zhang et al., 2011), the ubiquitin signal detected in *Arl6*$^{-/-}$
128 cilia may correspond to ubiquitin conjugated to SMO or GPR161. We detected a significant
129 elevation of the ciliary ubiquitin levels in *Arl6*$^{-/-}$ cells when treated with the SMO agonist SAG
130 (**Figure 1E-F**). Because SMO ubiquitination was previously shown to decrease upon its
131 activation (Xia et al., 2012; Jiang et al., 2019), it is likely that the elevated ciliary ubiquitin signal
132 detected in SAG-treated cells is associated with GPR161. As activation of SMO triggers exit of
133 GPR161 but this exit is frustrated when BBSome function goes awry, these data suggest that
134 GPR161 becomes ubiquitinated prior to its BBSome-dependent exit. Collectively, these data
135 suggest that GPCRs are ubiquitinated in a regulated fashion inside cilia and subsequently
136 retrieved into the cell by the BBSome.

137 To test the functional importance of GPCR ubiquitination in BBSome-mediated exit from cilia,
138 we removed all ubiquitination sites from SSTR3 and GPR161 by mutating all cytoplasm-

139 exposed lysine residues to arginine (cK0 variants). Exit kinetics were precisely monitored by real-
140 time tracking of individual cilia in live cells. In both cases, the cK0 variant underwent markedly
141 slower signal-dependent exit from cilia than the WT allele (**Figure 2A-B**). Measurement of exit
142 rates revealed that exit of SSTR3cK0 was ~2-fold slower than SSTR3 and that exit of
143 GPR161cK0 was ~2.5-fold slower than GPR161. The residual exit rates of the cK0 mutants
144 indicate the existence of alternative mechanisms of exit that complement GPCR ubiquitination
145 or bypass BBSome-dependent retrieval (see discussion).

146 To rule out that the observed ciliary exit defect of the cK0 mutants was an indirect consequence
147 of defective endocytosis for example because of clogging of the ciliary exit path, we directly
148 assessed endocytosis of SSTR3 and SSTR3cK0. The surface-exposed pool of $^{AP}$SSTR3 was pulse
149 labeled with fluorescently labeled monovalent streptavidin (mSA) and cells were stimulated with
150 sst. The faint hazy signal corresponding to the plasma membrane pool of SSTR3 disappeared
151 after 10 min in the presence of sst in a similar fashion for both WT and cK0 variants (**Figure**
152 **2C**). Concurrently, the WT and cK0 variants appeared in cytoplasmic foci corresponding to
153 endocytic vesicles (**Figure 2C**). Counting cytoplasmic foci revealed that endocytosis proceeded
154 normally irrespective of the ubiquitination competence of SSTR3 (**Figure 2D**). SSTR3 thus
155 behaves similarly to nearly every GPCR tested to date, in that it does not require ubiquitination
156 for its signal-dependent internalization. Indeed, while ubiquitination of plasma membrane
157 proteins is a major driver of internalization in yeast, ubiquitination of signaling receptors is
158 generally dispensable for signal-dependent internalization in mammalian cells (Dores and Trejo,
159 2019; Piper et al., 2014; Skieterska et al., 2017).

160 These results strongly support a direct role for GPCR ubiquitination in promoting signal-
161 dependent exit from cilia.

162

163 **Ciliary K63 ubiquitin linkages are required for GPCR exit**

164 We next sought to characterize the type of ubiquitin conjugates that are attached to ciliary
165 proteins. The FK1 and FK2 antibodies used in our immunofluorescent studies recognize

166 ubiquitin either as single adduct or in chain but not free ubiquitin (Fujimuro et al., 1994;
167 Emmerich and Cohen, 2015). The availability of antibodies specific for K48 and K63 ubiquitin
168 linkages (Newton et al., 2008) enabled us to determine the types of ubiquitin conjugates that are
169 attached to ciliary GPCRs. While we found no detectable signal for K48-linked ubiquitin chains
170 (UbK48) in cilia, the signal for K63-linked ubiquitin (UbK63) linkages mirrored the ciliary
171 response observed with the FK1 and FK2 antibody in IMCD3-[SSTR3] cells subjected to
172 agonist treatment (**Figure 3A-B and S1C-D**). Given the high specificity and selectivity of the
173 K48 and K63 linkage antibodies, these data strongly suggest that K63Ub chains are added onto
174 SSTR3 inside cilia upon activation.

175 To confirm that K63 of Ub is the main linkage used for the elongation of Ub chains on SSTR3,
176 we transfected variants of ubiquitin with lysines mutated to arginines into *Arl6*$^{-/-}$ cells stably
177 expressing SSTR3. Signal-dependent ubiquitination of SSTR3 was abrogated when all seven
178 lysines of Ub were mutated to arginines (**Figure 3C-D**). However, when K63 was the only lysine
179 left intact on Ub, signal-dependent ubiquitination of SSTR3 was restored to the same extent as
180 with WT Ub (**Figure 3C-D**). We conclude that UbK63 chains are assembled onto SSTR3 in
181 response to SSTR3 activation inside cilia.

182 To determine the functional importance of UbK63 linkages in tagging GPCRs for exit from cilia,
183 we sought to specifically interfere with UbK63 linkages inside cilia (**Figure 4A**). Structural and
184 biochemical studies have demonstrated that the deubiquitinase AMSH possesses a near-absolute
185 specificity for UbK63 linkages and does not cleave other Ub chain linkages or Ub-substrates
186 linkages (Sato et al., 2008; McCullough et al., 2004). AMSH normally function on the surface of
187 late endosomes in concert with the endosomal sorting complex required for transport (ESCRT)
188 protein STAM (McCullough et al., 2006). AMSH was previously fused to the epidermal growth
189 factor receptor EGFR to demonstrate that UbK63 chains assembled on EGFR are dispensable
190 for internalization but required for sorting into lysosomes (Huang et al., 2013). We targeted
191 AMSH to cilia using the well-validated ciliary targeting signal from the ciliopathy protein
192 NPHP3 (Nakata et al., 2012; Wright et al., 2011) and analyzed the exit of three distinct GPCRs:
193 SMO, GPR161 and SSTR3. To alleviate concerns related to the interaction of AMSH with the

194 STAM, we deleted the STAM-interacting domain of AMSH and only expressed the catalytic
195 domain of AMSH. The signal-dependent exit of SSTR3 was assessed by treating IMCD3-
196 [SSTR3] cells with sst for 2h. In cells expressing cilia-AMSH (a fusion of NPHP3[1-200] to GFP
197 and the catalytic domain of AMSH), sst no longer triggered a significant reduction in the ciliary
198 levels of SSTR3 (**Figure 4B-C**). Care was taken to only analyze cells that expressed modest
199 levels of cilia-AMSH as judged by GFP fluorescence (**Figure S3**). In contrast, SSTR3 exit
200 proceeded normally in cells that expressed NPHP3[1-200]-GFP alone or a catalytically dead
201 variant of cilia-AMSH that we named cilia-ASMH† (**Figure 4B-C**). These controls strongly
202 suggest that cilia-AMSH exerts its effects on SSTR3 exit by cleaving UbK63 chains inside cilia, a
203 conclusion borne out by imaging ciliary UbK63 in cells transfected with cilia-AMSH (**Figure**
204 **S4**). Similarly, the exit of endogenous GPR161 from RPE cell cilia upon activation of the
205 Hedgehog pathway was abolished in cells expressing moderate levels of cilia-AMSH (**Figure**
206 **4D-E**). Neither NPHP3[1-200]-GFP nor cilia-AMSH† blocked the signal-dependent exit of
207 GPR161 from cilia (**Figure 4D-E**).

208 Unlike GPR161 and other ciliary GPCRs such as the Somatostatin receptor 3 (SSTR3) that are
209 removed from cilia by the BBSome only when they become activated, SMO undergoes
210 constitutive BBSome-dependent exit from cilia in the absence of Hedgehog pathway stimulation
211 (Nachury, 2018; Ye et al., 2018; Ocbina and Anderson, 2008; Zhang et al., 2011). Signal-
212 dependent accumulation of SMO in cilia is achieved, at least in part, by suppression of its exit
213 (Milenkovic et al., 2015; Nachury and Mick, 2019; Ye et al., 2018). In cells expressing cilia-
214 AMSH, endogenous SMO spontaneously accumulated inside cilia in the absence of Hedgehog
215 pathway activation (**Figure 4F-G**). Again, neither NPHP3[1-200]-GFP nor cilia-AMSH†
216 influenced the ciliary accumulation of SMO (**Figure 4F-G**).

217 Together, these results indicate that K63-linked ubiquitin chains inside cilia, presumably built
218 onto each ciliary GPCRs under a specific signaling stimulus, are required for GPCR removal
219 from cilia.

220

221 **β-arrestin 2 mediates signal-dependent ubiquitination of ciliary GPCRs**

222 As β-arrestin 2 is required for signal-dependent exit of GPR161 and SSTR3 from cilia (Green et
223 al., 2015; Pal et al., 2016; Ye et al., 2018), we sought to determine the functional relationship
224 between β-arrestin 2 and the BBSome. As previously described (Green et al., 2015), β-arrestin 2
225 is initially undetectable inside cilia and becomes recruited to cilia within minutes of SSTR3
226 agonist addition (**Figure 5A-C**). The ciliary β-arrestin 2 signal reaches a plateau after about 10
227 min and the $t_{1/2}$ for ciliary accumulation is less than 5 min (**Figure 5C**). Meanwhile the $t_{1/2}$ for
228 BBSome recruitment to the tip of cilia was 10 min and the first signs of detectable SSTR3 exit
229 were seen between 10 and 15 min (**Figure 5C**). These kinetics suggested that β-arrestin 2 is first
230 recruited to activated ciliary SSTR3 before the BBSome ferries activated SSTR3 out of cilia.
231 When ARL6 was depleted, the basal levels of ciliary β-arrestin 2 were elevated but the kinetics of
232 β-arrestin 2 accumulation in cilia upon SSTR3 activation were indistinguishable from control-
233 depleted cells (**Figure 5A-B**). These data suggest that a small fraction of SSTR3 that is tonically
234 active fails to exit cilia in ARL6-depleted cells and recruits β-arrestin 2. From these data, we
235 conclude that β-arrestin 2 functions either upstream of, or in parallel with the BBSome in signal-
236 dependent retrieval of GPCRs. Similarly, the kinetics of GPR161 exit and β-arrestin 2 ciliary
237 recruitment upon activation of the Hh pathway indicated that β-arrestin 2 reaches its maximal
238 ciliary level before the first signs of GPR161 exit become evident (**Figure 5D**).

239 We previously proposed that β-arrestin 2 may bridge activated GPCRs to the BBSome (Ye et al.,
240 2018; Nachury, 2018). Yet, we have thus far failed to detect a biochemical interaction between β-
241 arrestin 2 and the BBSome. Furthermore, the continuous distribution patterns of β-arrestin 2 and
242 SSTR3 inside cilia are similar to one another and distinct from the discontinuous pattern of the
243 BBSome (**Figure 5A**), arguing against a direct association of β-arrestin 2 with BBSome/IFT
244 trains inside cilia. We considered the alternative hypothesis that β-arrestin 2 function upstream of
245 the BBSome. Given that β-arrestin 2 functions in the signal-dependent targeting of GPCRs from
246 the plasma membrane to the lysosome by recruiting ubiquitin ligases to activated GPCRs (Henry
247 et al., 2012; Bhandari et al., 2007; Shenoy et al., 2008; Martin et al., 2003), we posited that β-
248 arrestin 2 recognizes activated GPCRs inside cilia to direct their ubiquitination and subsequent

249 selection by the BBSome for removal from cilia. A central prediction of this model is that β-
250 arrestin 2 is required for the ubiquitination of ciliary GPCRs in response to stimulation. To test
251 this prediction, we deleted the β-arrestin 2 gene *Arrb2* in *Arl6* knockout IMCD3 cells (Nager et
252 al., 2017). While the signal-dependent exit of SSTR3 from cilia failed in both *Arl6*$^{-/-}$ and *Arl6*$^{-/-}$
253 *Arrb2*$^{-/-}$ cells (**Figures 1A-B and 6A-B**), ubiquitin staining in cilia and by inference signal-
254 dependent ubiquitination of SSTR3 was only observed in *Arl6*$^{-/-}$ cells (**Figures 6A-B**). In *Arl6*$^{-/-}$
255 *Arrb2*$^{-/-}$ cells, the signal-dependent increase in ciliary ubiquitin signal was no longer observed
256 (**Figures 6A-B**). Similarly, the increase in ciliary ubiquitin signal seen in *Arl6*$^{-/-}$ cells treated with
257 the Hedgehog pathway agonist SAG was no longer observed in the absence of β-arrestin 2
258 (**Figure 6C-D**). These data indicate that, in the absence of BBSome function, ciliary GPCRs
259 become ubiquitinated in response to activation in a β-arrestin 2-dependent manner. We sought
260 to confirm our imaging-based finding with a biochemical analysis of SSTR3 ubiquitination.
261 While SSTR3 ubiquitination was readily detected in *Arl6*$^{-/-}$ cells and measurably increased upon
262 stimulation with sst, the deletion of β-arrestin 2 in *Arl6*$^{-/-}$ cells drastically reduced SSTR3
263 ubiquitination levels and no sst-dependent increase of SSTR3 ubiquitination was detected in
264 *Arl6*$^{-/-}$ /*Arrb2*$^{-/-}$ cells (**Figure 6E-F**).

265 Together, these data suggest the following order of action: GPCR activation, β-arrestin 2
266 engagement, Ub ligase recruitment, assembly of K63Ub chains on the GPCR, and finally
267 selection of ubiquitinated GPCRs for BBSome-mediated retrieval (**Figure 7E**).

268

269 **Constitutively retrieved BBSome cargoes are ubiquitinated prior to exit**

270 Besides removing GPCRs from cilia in a regulated fashion, the BBSome also clears cilia of
271 unwanted proteins that accidentally enter cilia. In the single-cell flagellated organism
272 *Chlamydomonas reinhardtii*, mutations in the BBSome subunit Bbs4 cause a constitutive
273 accumulation of several proteins including Phospholipase D in cilia (Lechtreck et al., 2009).
274 When stained for ubiquitin, *Bbs4 Chlamydomonas* showed a 2-fold enrichment in ciliary signal
275 compared to WT (**Fig. 7A-B**). Isolation of cilia revealed the accumulation of ubiquitin

276 conjugates above 80 kDa in *Bbs4* mutant *Chlamydomonas* cilia (**Fig. 7C**). These results are
277 consistent with the hypothesis that ciliary proteins subject to constitutive retrieval are
278 ubiquitinated prior to their removal from cilia by the BBSome.

279 In the mammalian retina, proteomics studies have found over 100 proteins accumulating in the
280 outer segment (the equivalent of the cilium) of *Bbs* photoreceptors compared to WT
281 photoreceptors (Datta et al., 2015). When we stained sections of mouse retina for ubiquitin, we
282 found a drastic accumulation of ubiquitin signal in the outer segment of *Bbs4*$^{-/-}$ photoreceptors
283 compared to WT photoreceptors (**Fig. 7D**). We note that the nature of ubiquitin conjugates
284 remains to be determined in the case of constitutive cargoes. These results suggest that a variety
285 of proteins that accidentally flow into the photoreceptors outer segments –possibly caught on the
286 tremendous flux of rhodopsin trafficking to the outer segment (Baker et al., 2008)– are recognized
287 as foreign to the cilium, ubiquitinated on site and selected for removal by the BBSome (**Figure**
288 **7E**).

289 **DISCUSSION**

290 **Recognition of K63-linked ubiquitin chains by the ciliary exit machinery**

291 Our results indicate that K63-linked ubiquitin chains tag activated GPCRs and likely other
292 unwanted proteins for BBSome-mediated removal from cilia. Prior findings in trypanosomes
293 suggest that the BBSome may directly recognize ubiquitin (Langousis et al., 2016), although
294 direct biochemical evidence and information regarding ubiquitin chain specificity is still missing.
295 It is also known that the BBSome directly recognizes cytoplasmic determinants in the GPCRs it
296 ferries out of cilia (Jin et al., 2010; Klink et al., 2017; Ye et al., 2018; Seo et al., 2011; Domire et
297 al., 2011). We propose that the summation of weak molecular interactions between the BBSome
298 and UbK63 chains on one hand and the BBSome and GPCRs cytoplasmic loops on the other
299 hand increases the BBSome-cargo interaction to enable sorting of ubiquitinated GPCRs out of
300 cilia. In support of this bivalent recognition of ubiquitinated cargoes by the BBSome, the affinity
301 of the BBSome for cytoplasmic determinant of GPCRs are in the μM range (Klink et al., 2017)
302 and affinities of ubiquitin-binding proteins for ubiquitin typically reside in the sub mM range
303 (Husnjak and Dikic, 2012). The nature of the biochemical entity that directly recognizes
304 ubiquitin, and in particular UbK63 chains remains to be determined: while the BBSome was
305 pulled down on Ub-agarose resin from trypanosome lysates (Langousis et al., 2016), no known
306 Ub-binding domain is found in the BBSome polypeptides. Furthermore, the IFT-A subunit IFT-
307 139 associates with ubiquitinated α-tubulin in ciliary extracts from *Chlamydomonas*, suggesting a
308 possible recognition of ubiquitin by IFT139 (Wang et al., 2019). Again, the absence of known
309 Ub-binding domain in the sequence of IFT139 presents a challenge to this hypothesis.

310

311 **Requirements for K63-linked ubiquitination in ciliary exit and sorting to the**
312 **lysosome**

313 Wang et al. (2019) found that α-tubulin is modified by UbK63 chains and not UbK48 chain
314 upon ciliary disassembly. The ubiquitin ligases that have been associated with ciliary clearance of
315 Patched 1 and of PDGFRαα specifically assemble UbK63 chains (Kim et al., 2015; Yue et al.,

316 2014; Schmid et al., 2018). The suppression of GPR161, SSTR3 and SMO exit by cilia-AMSH
317 (**Figure 4**) demonstrates that UbK63 chains are recognized inside cilia to direct trafficking out of
318 cilia. The milder exit defect observed when acceptor lysines are mutated on ciliary GPCRs
319 (**Figure 2**) than when cilia-AMSH is expressed (**Figure 4**) suggests that K63Ub chains added
320 onto other ciliary proteins besides GPCRs may participate in ciliary exit. A role for
321 ubiquitination of the ciliary transport machinery in exit is in line with the functional importance
322 of ubiquitination of the endolysosomal machinery in GPCR trafficking (Dores and Trejo, 2019).
323 β arrestin ubiquitination promotes internalization of the $\beta_2$-adrenergic receptor ($\beta_2$AR) (Shenoy
324 et al., 2001, 2007; Shenoy and Lefkowitz, 2003), ubiquitination of the ESCRT components Hrs
325 and STAM participates in sorting of the chemokine receptor CXCR4 into the MVB (Malik and
326 Marchese, 2010; Marchese et al., 2003) and ubiquitination of the ESCRT-III recruitment factor
327 ALIX enhances MVB sorting of the protease activated receptor PAR-1 (Dores et al., 2015).

328 The requirement for UbK63 chains in signal-dependent exit from the cilium contrasts with the
329 more limited role of ubiquitin and UbK63 chains in signal-dependent endocytosis of signaling
330 receptors at the plasma membrane in mammals. Although ubiquitination is a major driver of
331 endocytosis in yeast (Stringer and Piper, 2011; Piper et al., 2014), foundational studies on
332 epidermal growth factor receptor (EGFR) trafficking found that signal-dependent receptor
333 ubiquitination is not essential for internalization because it is redundant with other
334 internalization mechanisms (Goh et al., 2010; Huang et al., 2013; Fortian et al., 2015). Studies of
335 an EGFR-AMSH fusion found that UbK63 chains attached onto EGFR become increasingly
336 necessary as EGFR progresses along the degradative route and a strict requirement for K63-
337 linked ubiquitin chains is observed at the terminal step of EGFR sorting into the lumen of
338 multivesicular body (MVB) (Huang et al., 2013). A strict requirement for receptor ubiquitination
339 in degradative sorting but not in internalization can be generalized to nearly all GPCRs
340 (Skieterska et al., 2017), namely $\beta_2$AR (Shenoy et al., 2001), CXCR4 (Marchese and Benovic,
341 2001), μ opioid receptor (Hislop et al., 2011), κ opioid receptor (Li et al., 2008), δ opioid receptor
342 (Henry et al., 2011), neurokinin-1 receptor (Cottrell et al., 2006), protease activated receptor 2
343 (PAR-2) (Jacob et al., 2005) and vasopressin receptor 2 (V2R) (Martin et al., 2003). Similarly, we

344 find that SSTR3 endocytosis proceeds normally in the absence of SSTR3 ubiquitination (**Figure**
345 **2C-D**). Studying the importance of ubiquitin K63 in mammalian cells via genetics remains
346 challenging because of the multiple genes encoding Ub but in yeast strains expressing UbK63R
347 as the sole source of Ub, the Gap1 permease is internalized normally and fails to get sorted into
348 the MVB (Lauwers et al., 2009).

349 The parallels between sorting at the late endosome and ciliary trafficking extend to β arrestin-
350 directed ubiquitination. While β arrestin functions inside cilia to direct the addition of ubiquitin
351 onto activated SSTR3 and GPR161 (**Figures 5 and 6**), β arrestin-mediated ubiquitination
352 selectively affects sorting at the level of endosomes rather that at the plasma membrane for
353 activated CXCR4 (Bhandari et al., 2007), $\beta_2$AR (Shenoy et al., 2008) and V2R (Martin et al.,
354 2003) and β arrestin-mediated ubiquitination of CXCR4 was shown to take place on endosomes
355 (Malik and Marchese, 2010). In this context, the recognition of K63-linked ubiquitin chain inside
356 cilia may befit the endosomal origin of primary cilia (Sorokin, 1962; Westlake et al., 2011;
357 Mitchell, 2017).

358 The parallels between endosomal and ciliary trafficking lead us to speculate that some
359 ubiquitinated proteins might be accidentally sorted to cilia instead of late endosomes. These
360 proteins would then need to be retrieved from cilia by the BBSome. Thus, the Ub signal detected
361 in photoreceptor outer segment and in *Chlamydomonas* flagella might result from the accidental
362 import of ubiquitinated proteins into cilia rather than *in situ* ubiquitination of unwanted proteins
363 inside cilia.

364

365 **Potential coupling between BBSome-mediated exit and degradative sorting**

366 An interesting consideration is the relationship between ciliary exit and endo-lysosomal sorting. It
367 has been proposed that endocytosis of signaling receptors is intimately coupled to their exit from
368 cilia (Pedersen et al., 2016). However, single molecule imaging of GPR161 exiting cilia suggests
369 that activated GPR161 diffuses into the plasma membrane after it exits from the ciliary
370 compartment (Ye et al., 2018). Prior findings that worm mutants for BBSome or the ESCRT

371 machinery both fail to remove ciliary proteins fused to Ub from cilia (Hu et al., 2007; Xu et al.,
372 2015) suggest the provocative possibility that ciliary exit may be tightly coupled to degradative
373 sorting. Nonetheless, the hypothesis that interfering with UbK63 chain formation on ciliary
374 GPCRs indirectly blocks ciliary exit because of a primary defect in endocytosis can be rejected
375 because ubiquitination is not a major determinant of SSTR3 endocytosis and because cilia-
376 AMSH potently and specifically blocks the signal-dependent exit of ciliary GPCRs.

377 In this context, the contrast between the dramatic increase in ubiquitinated SSTR3 levels in *Arl6*$^{-/-}$
378 cells compared to WT cells even in the absence of stimulation (**Figure 1C-D**) and the modest
379 increase in ciliary Ub levels in *Arl6*$^{-/-}$ cells compared to WT cells in the absence of stimulation
380 (**Figure 1A-B**) suggests that a considerable amount of ubiquitinated SSTR3 accumulates outside
381 of cilia in *Arl6*$^{-/-}$ cells. One interpretation consistent with a direct coupling between ciliary exit
382 and degradation is that a small fraction of ubiquitinated SSTR3 escapes cilia in *Arl6*$^{-/-}$ cells but
383 fails to reach to correct degradative route. In this interpretation, the BBSome would deliver its
384 cargoes to the ESCRT machinery for routing into the lysosomal degradative pathway.

385

386 **Ubiquitination and control of the ciliary proteome**

387 A role for ubiquitination in selecting unwanted proteins for removal from cilia may unify the
388 functions of the BBSome in signal-dependent retrieval of GPCRs and the constitutive clearance
389 of proteins that accidentally enter cilia. In both of these cases, unwanted ciliary proteins need to
390 be recognized as 'non-self' by a ciliary surveillance machinery. For GPCRs, β arrestin orchestrate
391 the recognition of activated GPCRs as unwanted by directing their ubiquitination. A fascinating
392 question for future investigations is how the more than 100 proteins that accumulate in outer
393 segments of *Bbs* photoreceptors are recognized as 'non-self' and tagged with ubiquitin.
394

395 **REFERENCES**


396 Anvarian, Z., K. Mykytyn, S. Mukhopadhyay, L.B. Pedersen, and S.T. Christensen. 2019.
397 Cellular signalling by primary cilia in development, organ function and disease. *Nat. Rev.*
398 *Nephrol.* doi:10.1038/s41581-019-0116-9.

399 Baker, S.A., M. Haeri, P. Yoo, S.M. Gospe, N.P. Skiba, B.E. Knox, and V.Y. Arshavsky. 2008.
400 The outer segment serves as a default destination for the trafficking of membrane proteins
401 in photoreceptors. *J. Cell Biol.* 183:485–498. doi:10.1083/jcb.200806009.

402 Bhandari, D., J. Trejo, J.L. Benovic, and A. Marchese. 2007. Arrestin-2 interacts with the
403 ubiquitin-protein isopeptide ligase atrophin-interacting protein 4 and mediates
404 endosomal sorting of the chemokine receptor CXCR4. *J. Biol. Chem.* 282:36971–36979.
405 doi:10.1074/jbc.M705085200.

406 Chiang, A.P., J.S. Beck, H. Yen, M.K. Tayeh, T.E. Scheetz, R.E. Swiderski, D.Y. Nishimura,
407 T.A. Braun, K.-Y.A. Kim, J. Huang, K. Elbedour, R. Carmi, D.C. Slusarski, T.L.
408 Casavant, E.M. Stone, and V.C. Sheffield. 2006. Homozygosity mapping with SNP
409 arrays identifies TRIM32, an E3 ubiquitin ligase, as a Bardet-Biedl syndrome gene
410 (BBS11). *Proc. Natl. Acad. Sci. U. S. A.* 103:6287–6292. doi:10.1073/pnas.0600158103.

411 Corbit, K.C., P. Aanstad, V. Singla, A.R. Norman, D.Y.R. Stainier, and J.F. Reiter. 2005.
412 Vertebrate Smoothened functions at the primary cilium. *Nature*. 437:1018–1021.
413 doi:10.1038/nature04117.

414 Cottrell, G.S., B. Padilla, S. Pikios, D. Roosterman, M. Steinhoff, D. Gehringer, E.F. Grady, and
415 N.W. Bunnett. 2006. Ubiquitin-dependent Down-regulation of the Neurokinin-1
416 Receptor. *J. Biol. Chem.* 281:27773–27783. doi:10.1074/jbc.M603369200.

417 Craige, B., J.M. Brown, and G.B. Witman. 2013. Isolation of Chlamydomonas Flagella. *Curr.*
418 *Protoc. Cell Biol.* 59:3.41.1-3.41.9. doi:10.1002/0471143030.cb0341s59.

419 Datta, P., C. Allamargot, J.S. Hudson, E.K. Andersen, S. Bhattarai, A.V. Drack, V.C. Sheffield,
420 and S. Seo. 2015. Accumulation of non-outer segment proteins in the outer segment
421 underlies photoreceptor degeneration in Bardet-Biedl syndrome. *Proc Natl Acad Sci U A*.
422 112:E4400–9. doi:10.1073/pnas.1510111112.

423 Domire, J.S., J.A. Green, K.G. Lee, A.D. Johnson, C.C. Askwith, and K. Mykytyn. 2011.
424 Dopamine receptor 1 localizes to neuronal cilia in a dynamic process that requires the
425 Bardet-Biedl syndrome proteins. *Cell. Mol. Life Sci. CMLS*. 68:2951–2960.
426 doi:10.1007/s00018-010-0603-4.

427 Dores, M.R., H. Lin, N. J Grimsey, F. Mendez, and J. Trejo. 2015. The α-arrestin ARRDC3
428 mediates ALIX ubiquitination and G protein-coupled receptor lysosomal sorting. *Mol.*
429 *Biol. Cell.* 26:4660–4673. doi:10.1091/mbc.E15-05-0284.

430 Dores, M.R., and J. Trejo. 2019. Endo-lysosomal sorting of G-protein-coupled receptors by
431 ubiquitin: Diverse pathways for G-protein-coupled receptor destruction and beyond.
432 *Traffic Cph. Den.* 20:101–109. doi:10.1111/tra.12619.

433 Emmerich, C.H., and P. Cohen. 2015. Optimising methods for the preservation, capture and
434 identification of ubiquitin chains and ubiquitylated proteins by immunoblotting. *Biochem.*
435 *Biophys. Res. Commun.* 466:1–14. doi:10.1016/j.bbrc.2015.08.109.

436 Fortian, A., L.K. Dionne, S.H. Hong, W. Kim, S.P. Gygi, S.C. Watkins, and A. Sorkin. 2015.
437 Endocytosis of Ubiquitylation-Deficient EGFR Mutants via Clathrin-Coated Pits is
438 Mediated by Ubiquitylation. *Traffic Cph. Den.* 16:1137–1154. doi:10.1111/tra.12314.

439 Fujimuro, M., H. Sawada, and H. Yokosawa. 1994. Production and characterization of
440 monoclonal antibodies specific to multi-ubiquitin chains of polyubiquitinated proteins.
441 *FEBS Lett.* 349:173–180. doi:10.1016/0014-5793(94)00647-4.

442 Gigante, E.D., and T. Caspary. 2020. Signaling in the primary cilium through the lens of the
443 Hedgehog pathway. *Wiley Interdiscip. Rev. Dev. Biol.* e377. doi:10.1002/wdev.377.

444 Goh, L.K., F. Huang, W. Kim, S. Gygi, and A. Sorkin. 2010. Multiple mechanisms collectively
445 regulate clathrin-mediated endocytosis of the epidermal growth factor receptor. *J. Cell*
446 *Biol.* 189:871–883. doi:10.1083/jcb.201001008.

447 Gorman, D.S., and R.P. Levine. 1965. Cytochrome f and plastocyanin: their sequence in the
448 photosynthetic electron transport chain of Chlamydomonas reinhardi. *Proc. Natl. Acad. Sci.*
449 *U. S. A.* 54:1665–1669. doi:10.1073/pnas.54.6.1665.

450 Green, J.A., C.L. Schmid, E. Bley, P.C. Monsma, A. Brown, L.M. Bohn, and K. Mykytyn. 2015.
451 Recruitment of β-Arrestin into Neuronal Cilia Modulates Somatostatin Receptor
452 Subtype 3 Ciliary Localization. *Mol. Cell. Biol.* 36:223–235. doi:10.1128/MCB.00765-15.

453 Haglund, K., S. Sigismund, S. Polo, I. Szymkiewicz, P.P. Di Fiore, and I. Dikic. 2003. Multiple
454 monoubiquitination of RTKs is sufficient for their endocytosis and degradation. *Nat. Cell*
455 *Biol.* 5:461–466. doi:10.1038/ncb983.

456 Henry, A.G., J.N. Hislop, J. Grove, K. Thorn, M. Marsh, and M. von Zastrow. 2012.
457 Regulation of endocytic clathrin dynamics by cargo ubiquitination. *Dev. Cell.* 23:519–532.
458 doi:10.1016/j.devcel.2012.08.003.

459 Henry, A.G., I.J. White, M. Marsh, M. von Zastrow, and J.N. Hislop. 2011. The Role of
460 Ubiquitination in Lysosomal Trafficking of δ-Opioid Receptors. *Traffic*. 12:170–184.
461 doi:10.1111/j.1600-0854.2010.01145.x.

462 Hislop, J.N., A.G. Henry, and M. von Zastrow. 2011. Ubiquitination in the first cytoplasmic loop
463 of μ-opioid receptors reveals a hierarchical mechanism of lysosomal down-regulation. *J.*
464 *Biol. Chem.* 286:40193–40204. doi:10.1074/jbc.M111.288555.

465 Howarth, M., and A.Y. Ting. 2008. Imaging proteins in live mammalian cells with biotin ligase
466 and monovalent streptavidin. *Nat. Protoc.* 3:534–545. doi:10.1038/nprot.2008.20.

467 Hu, J., S.G. Wittekind, and M.M. Barr. 2007. STAM and Hrs down-regulate ciliary TRP
468 receptors. *Mol. Biol. Cell.* 18:3277–3289. doi:10.1091/mbc.E07-03-0239.

469 Huang, F., X. Zeng, W. Kim, M. Balasubramani, A. Fortian, S.P. Gygi, N.A. Yates, and A.
470 Sorkin. 2013. Lysine 63-linked polyubiquitination is required for EGF receptor
471 degradation. *Proc. Natl. Acad. Sci.* 110:15722–15727. doi:10.1073/pnas.1308014110.

472 Huang, K., D.R. Diener, and J.L. Rosenbaum. 2009. The ubiquitin conjugation system is
473 involved in the disassembly of cilia and flagella. *J. Cell Biol.* 186:601–613.
474 doi:10.1083/jcb.200903066.

475 Husnjak, K., and I. Dikic. 2012. Ubiquitin-binding proteins: decoders of ubiquitin-mediated
476 cellular functions. *Annu. Rev. Biochem.* 81:291–322. doi:10.1146/annurev-biochem-
477 051810-094654.

478 Jacob, C., G.S. Cottrell, D. Gehringer, F. Schmidlin, E.F. Grady, and N.W. Bunnett. 2005. c-
479 Cbl mediates ubiquitination, degradation, and down-regulation of human protease-
480 activated receptor 2. *J. Biol. Chem.* 280:16076–16087. doi:10.1074/jbc.M500109200.

481 Jiang, W., X. Yao, Z. Shan, W. Li, Y. Gao, and Q. Zhang. 2019. E3 ligase Herc4 regulates
482 Hedgehog signalling through promoting Smoothened degradation. *J. Mol. Cell Biol.*
483 11:791–803. doi:10.1093/jmcb/mjz024.

484 Jin, H., S.R. White, T. Shida, S. Schulz, M. Aguiar, S.P. Gygi, J.F. Bazan, and M.V. Nachury.
485 2010. The conserved Bardet-Biedl syndrome proteins assemble a coat that traffics
486 membrane proteins to cilia. *Cell.* 141:1208–1219. doi:10.1016/j.cell.2010.05.015.

487 Kim, J., E.Y. C Hsia, A. Brigui, A. Plessis, P.A. Beachy, and X. Zheng. 2015. The role of ciliary
488 trafficking in Hedgehog receptor signaling. *Sci. Signal.* 8:ra55–ra55.
489 doi:10.1126/scisignal.aaa5622.

490 Klink, B.U., E. Zent, P. Juneja, A. Kuhlee, S. Raunser, and A. Wittinghofer. 2017. A
491 recombinant BBSome core complex and how it interacts with ciliary cargo. *eLife*. 6.
492 doi:10.7554/eLife.27434.

493 Langousis, G., M.M. Shimogawa, E.A. Saada, A.A. Vashisht, R. Spreafico, A.R. Nager, W.D.
494 Barshop, M.V. Nachury, J.A. Wohlschlegel, and K.L. Hill. 2016. Loss of the BBSome
495 perturbs endocytic trafficking and disrupts virulence of Trypanosoma brucei. *Proc Natl*
496 *Acad Sci U A*. 113:632–637. doi:10.1073/pnas.1518079113.

497 Lauwers, E., C. Jacob, and B. André. 2009. K63-linked ubiquitin chains as a specific signal for
498 protein sorting into the multivesicular body pathway. *J. Cell Biol.* 185:493–502.
499 doi:10.1083/jcb.200810114.

500 Lechtreck, K.-F., E.C. Johnson, T. Sakai, D. Cochran, B.A. Ballif, J. Rush, G.J. Pazour, M.
501 Ikebe, and G.B. Witman. 2009. The Chlamydomonas reinhardtii BBSome is an IFT
502 cargo required for export of specific signaling proteins from flagella. *J. Cell Biol.*
503 187:1117–1132. doi:10.1083/jcb.200909183.

504 Li, J.-G., D.S. Haines, and L.-Y. Liu-Chen. 2008. Agonist-Promoted Lys63-Linked
505 Polyubiquitination of the Human κ-Opioid Receptor Is Involved in Receptor Down-
506 Regulation. *Mol. Pharmacol.* 73:1319–1330. doi:10.1124/mol.107.042846.

507 Liew, G.M., F. Ye, A.R. Nager, J.P. Murphy, J.S. Lee, M. Aguiar, D. Breslow, S.P. Gygi, and
508 M.V. Nachury. 2014. The intraflagellar transport protein IFT27 promotes BBSome exit
509 from cilia through the GTPase ARL6/BBS3. *Dev. Cell*. 31:265–278.
510 doi:10.1016/j.devcel.2014.09.004.

511 Loktev, A.V., and P.K. Jackson. 2013. Neuropeptide Y family receptors traffic via the Bardet-
512 Biedl syndrome pathway to signal in neuronal primary cilia. *Cell Rep.* 5:1316–1329.
513 doi:10.1016/j.celrep.2013.11.011.

514 Malik, R., and A. Marchese. 2010. Arrestin-2 interacts with the endosomal sorting complex
515 required for transport machinery to modulate endosomal sorting of CXCR4. *Mol. Biol.*
516 *Cell*. 21:2529–2541. doi:10.1091/mbc.e10-02-0169.

517 Marchese, A., and J.L. Benovic. 2001. Agonist-promoted ubiquitination of the G protein-coupled
518 receptor CXCR4 mediates lysosomal sorting. *J. Biol. Chem.* 276:45509–45512.
519 doi:10.1074/jbc.C100527200.

520 Marchese, A., C. Raiborg, F. Santini, J.H. Keen, H. Stenmark, and J.L. Benovic. 2003. The E3
521 ubiquitin ligase AIP4 mediates ubiquitination and sorting of the G protein-coupled
522 receptor CXCR4. *Dev. Cell*. 5:709–722. doi:10.1016/s1534-5807(03)00321-6.

523 Martin, N.P., R.J. Lefkowitz, and S.K. Shenoy. 2003. Regulation of V2 Vasopressin Receptor
524 Degradation by Agonist-promoted Ubiquitination. *J. Biol. Chem.* 278:45954–45959.
525 doi:10.1074/jbc.M308285200.

526 McCullough, J., M.J. Clague, and S. Urbé. 2004. AMSH is an endosome-associated ubiquitin
527 isopeptidase. *J. Cell Biol.* 166:487–492. doi:10.1083/jcb.200401141.

528 McCullough, J., P.E. Row, Ó. Lorenzo, M. Doherty, R. Beynon, M.J. Clague, and S. Urbé.
529 2006. Activation of the Endosome-Associated Ubiquitin Isopeptidase AMSH by STAM,
530 a Component of the Multivesicular Body-Sorting Machinery. *Curr. Biol.* 16:160–165.
531 doi:10.1016/j.cub.2005.11.073.

532 Michel, M.A., P.R. Elliott, K.N. Swatek, M. Simicek, J.N. Pruneda, J.L. Wagstaff, S.M.V.
533 Freund, and D. Komander. 2015. Assembly and specific recognition of k29- and k33-
534 linked polyubiquitin. *Mol. Cell.* 58:95–109. doi:10.1016/j.molcel.2015.01.042.

535 Milenkovic, L., L.E. Weiss, J. Yoon, T.L. Roth, Y.S. Su, S.J. Sahl, M.P. Scott, and W.E.
536 Moerner. 2015. Single-molecule imaging of Hedgehog pathway protein Smoothened in
537 primary cilia reveals binding events regulated by Patched1. *Proc Natl Acad Sci U A.*
538 112:8320–8325. doi:10.1073/pnas.1510094112.

539 Mitchell, D.R. 2017. Evolution of Cilia. *Cold Spring Harb. Perspect. Biol.* 9:a028290.
540 doi:10.1101/cshperspect.a028290.

541 Mukhopadhyay, S., X. Wen, N. Ratti, A. Loktev, L. Rangell, S.J. Scales, and P.K. Jackson.
542 2013. The ciliary G-protein-coupled receptor Gpr161 negatively regulates the Sonic
543 hedgehog pathway via cAMP signaling. *Cell.* 152:210–223.
544 doi:10.1016/j.cell.2012.12.026.

545 Mykytyn, K., and C. Askwith. 2017. G-Protein-Coupled Receptor Signaling in Cilia. *Cold Spring*
546 *Harb. Perspect. Biol.* a028183. doi:10.1101/cshperspect.a028183.

547 Mykytyn, K., R.F. Mullins, R.F. Mullins, M. Andrews, M. Andrews, A.P. Chiang, A.P. Chiang,
548 R.E. Swiderski, R.E. Swiderski, B. Yang, B. Yang, T. Braun, T. Braun, T. Casavant, T.
549 Casavant, E.M. Stone, E.M. Stone, and V.C. Sheffield. 2004. Bardet-Biedl syndrome
550 type 4 (BBS4)-null mice implicate Bbs4 in flagella formation but not global cilia assembly.
551 *Proc. Natl. Acad. Sci. U. S. A.* 101:8664–8669. doi:10.1073/pnas.0402354101.

552 Nachury, M.V. 2018. The molecular machines that traffic signaling receptors into and out of
553 cilia. *Curr. Opin. Cell Biol.* 51:124–131. doi:10.1016/j.ceb.2018.03.004.

554 Nachury, M.V., and D.U. Mick. 2019. Establishing and regulating the composition of cilia for
555 signal transduction. *Nat. Rev. Mol. Cell Biol.* 20:389–405. doi:10.1038/s41580-019-0116-4.

556 Nager, A.R., J.S. Goldstein, V. Herranz-Pérez, D. Portran, F. Ye, J.M. García-Verdugo, and
557 M.V. Nachury. 2017. An Actin Network Dispatches Ciliary GPCRs into Extracellular
558 Vesicles to Modulate Signaling. *Cell.* 168:252–263.e14. doi:10.1016/j.cell.2016.11.036.

559 Nakata, K., D. Shiba, D. Kobayashi, and T. Yokoyama. 2012. Targeting of Nphp3 to the
560 primary cilia is controlled by an N-terminal myristoylation site and coiled-coil domains.
561 *Cytoskelet. Hoboken NJ.* 69:221–234. doi:10.1002/cm.21014.

562 Newton, K., M.L. Matsumoto, I.E. Wertz, D.S. Kirkpatrick, J.R. Lill, J. Tan, D. Dugger, N.
563 Gordon, S.S. Sidhu, F.A. Fellouse, L. Komuves, D.M. French, R.E. Ferrando, C. Lam,
564 D. Compaan, C. Yu, I. Bosanac, S.G. Hymowitz, R.F. Kelley, and V.M. Dixit. 2008.
565 Ubiquitin chain editing revealed by polyubiquitin linkage-specific antibodies. *Cell.*
566 134:668–678. doi:10.1016/j.cell.2008.07.039.

567 Ocbina, P.J.R., and K.V. Anderson. 2008. Intraflagellar transport, cilia, and mammalian
568 Hedgehog signaling: analysis in mouse embryonic fibroblasts. *Dev. Dyn.* 237:2030–2038.
569 doi:10.1002/dvdy.21551.

570 Pal, K., S. Hwang, B. Somatilaka, H. Badgandi, P.K. Jackson, K. DeFea, and S.
571 Mukhopadhyay. 2016. Smoothened determines β-arrestin-mediated removal of the G
572 protein-coupled receptor Gpr161 from the primary cilium. *J. Cell Biol.* 212:861–875.
573 doi:10.1083/jcb.201506132.

574 Pedersen, L.B., J.B. Mogensen, and S.T. Christensen. 2016. Endocytic Control of Cellular
575 Signaling at the Primary Cilium. *Trends Biochem. Sci.* 41:784–797.
576 doi:10.1016/j.tibs.2016.06.002.

577 Piper, R.C., I. Dikic, and G.L. Lukacs. 2014. Ubiquitin-Dependent Sorting in Endocytosis. *Cold*
578 *Spring Harb. Perspect. Biol.* 6:a016808–a016808. doi:10.1101/cshperspect.a016808.

579 Postma, M., and J. Goedhart. 2019. PlotsOfData-A web app for visualizing data together with
580 their summaries. *PLoS Biol.* 17:e3000202. doi:10.1371/journal.pbio.3000202.

581 Rohatgi, R., L. Milenkovic, and M.P. Scott. 2007. Patched1 regulates hedgehog signaling at the
582 primary cilium. *Sci. N. Y. NY.* 317:372–376. doi:10.1126/science.1139740.

583 Sato, Y., A. Yoshikawa, A. Yamagata, H. Mimura, M. Yamashita, K. Ookata, O. Nureki, K.
584 Iwai, M. Komada, and S. Fukai. 2008. Structural basis for specific cleavage of Lys 63-
585 linked polyubiquitin chains. *Nature.* 455:358–362. doi:10.1038/nature07254.

586 Schmid, F.M., K.B. Schou, M.J. Vilhelm, M.S. Holm, L. Breslin, P. Farinelli, L.A. Larsen, J.S.
587 Andersen, L.B. Pedersen, and S.T. Christensen. 2018. IFT20 modulates ciliary PDGFRα
588 signaling by regulating the stability of Cbl E3 ubiquitin ligases. *J. Cell Biol.* 217:151–161.
589 doi:10.1083/jcb.201611050.

590 Seo, S., Q. Zhang, K. Bugge, D. Breslow, C.C. Searby, M.V. Nachury, and V.C. Sheffield.
591 2011. A novel protein LZTFL1 regulates ciliary trafficking of the BBSome and
592 Smoothened. *PLoS Genet.* 7:e1002358. doi:10.1371/journal.pgen.1002358.

593 Shaner, N.C., G.G. Lambert, A. Chammas, Y. Ni, P.J. Cranfill, M.A. Baird, B.R. Sell, J.R.
594 Allen, R.N. Day, M. Israelsson, M.W. Davidson, and J. Wang. 2013. A bright
595 monomeric green fluorescent protein derived from Branchiostoma lanceolatum. *Nat.*
596 *Methods*. 10:407–409. doi:10.1038/nmeth.2413.

597 Shankar, H., H. Shankar, A. Michal, A. Michal, R.C. Kern, R.C. Kern, D.S. Kang, D.S. Kang,
598 V.V. Gurevich, V.V. Gurevich, and J.L. Benovic. 2010. Non-visual arrestins are
599 constitutively associated with the centrosome and regulate centrosome function. *J. Biol.*
600 *Chem.* 285:8316–8329. doi:10.1074/jbc.M109.062521.

601 Shearer, R.F., and D.N. Saunders. 2016. Regulation of primary cilia formation by the ubiquitin-
602 proteasome system. *Biochem. Soc. Trans.* 44:1265–1271. doi:10.1042/BST20160174.

603 Shenoy, S.K., L.S. Barak, K. Xiao, S. Ahn, M. Berthouze, A.K. Shukla, L.M. Luttrell, and R.J.
604 Lefkowitz. 2007. Ubiquitination of beta-arrestin links seven-transmembrane receptor
605 endocytosis and ERK activation. *J. Biol. Chem.* 282:29549–29562.
606 doi:10.1074/jbc.M700852200.

607 Shenoy, S.K., and R.J. Lefkowitz. 2003. Trafficking Patterns of β-Arrestin and G Protein-
608 coupled Receptors Determined by the Kinetics of β-Arrestin Deubiquitination. *J. Biol.*
609 *Chem.* 278:14498–14506. doi:10.1074/jbc.M209626200.

610 Shenoy, S.K., P.H. McDonald, T.A. Kohout, and R.J. Lefkowitz. 2001. Regulation of receptor
611 fate by ubiquitination of activated beta 2-adrenergic receptor and beta-arrestin. *Science*.
612 294:1307–1313. doi:10.1126/science.1063866.

613 Shenoy, S.K., K. Xiao, V. Venkataramanan, P.M. Snyder, N.J. Freedman, and A.M. Weissman.
614 2008. Nedd4 mediates agonist-dependent ubiquitination, lysosomal targeting, and
615 degradation of the beta2-adrenergic receptor. *J. Biol. Chem.* 283:22166–22176.
616 doi:10.1074/jbc.M709668200.

617 Skieterska, K., P. Rondou, and K. Van Craenenbroeck. 2017. Regulation of G Protein-Coupled
618 Receptors by Ubiquitination. *Int. J. Mol. Sci.* 18. doi:10.3390/ijms18050923.

619 Sorokin, S. 1962. Centrioles and the formation of rudimentary cilia by fibroblasts and smooth
620 muscle cells. *J. Cell Biol.* 15:363–377. doi:10.1083/jcb.15.2.363.

621 Stringer, D.K., and R.C. Piper. 2011. A single ubiquitin is sufficient for cargo protein entry into
622 MVBs in the absence of ESCRT ubiquitination. *J. Cell Biol.* 192:229–242.
623 doi:10.1083/jcb.201008121.

624 Swatek, K.N., and D. Komander. 2016. Ubiquitin modifications. *Cell Res.* 26:399–422.
625 doi:10.1038/cr.2016.39.

626 Wang, Q., Z. Peng, H. Long, X. Deng, and K. Huang. 2019. Polyubiquitylation of α-tubulin at
627 K304 is required for flagellar disassembly in Chlamydomonas. *J. Cell Sci.* 132.
628 doi:10.1242/jcs.229047.

629 Westlake, C.J., L.M. Baye, M.V. Nachury, K.J. Wright, K.E. Ervin, L. Phu, C. Chalouni, J.S.
630 Beck, D.S. Kirkpatrick, D.C. Slusarski, V.C. Sheffield, R.H. Scheller, and P.K. Jackson.
631 2011. Primary cilia membrane assembly is initiated by Rab11 and transport protein
632 particle II (TRAPPII) complex-dependent trafficking of Rabin8 to the centrosome. *Proc*
633 *Natl Acad Sci U A.* 108:2759–2764. doi:10.1073/pnas.1018823108.

634 Wingfield, J.L., K.-F. Lechtreck, and E. Lorentzen. 2018. Trafficking of ciliary membrane
635 proteins by the intraflagellar transport/BBSome machinery. *Essays Biochem.* 62:753–763.
636 doi:10.1042/EBC20180030.

637 Wright, K.J., L.M. Baye, A. Olivier-Mason, S. Mukhopadhyay, L. Sang, M. Kwong, W. Wang,
638 P.R. Pretorius, V.C. Sheffield, P. Sengupta, D.C. Slusarski, and P.K. Jackson. 2011. An
639 ARL3-UNC119-RP2 GTPase cycle targets myristoylated NPHP3 to the primary cilium.
640 *Genes Dev.* 25:2347–2360. doi:10.1101/gad.173443.111.

641 Xia, R., H. Jia, J. Fan, Y. Liu, and J. Jia. 2012. USP8 promotes smoothened signaling by
642 preventing its ubiquitination and changing its subcellular localization. *PLoS Biol.*
643 10:e1001238. doi:10.1371/journal.pbio.1001238.

644 Xu, Q., Y. Zhang, Q. Wei, Y. Huang, Y. Li, K. Ling, and J. Hu. 2015. BBS4 and BBS5 show
645 functional redundancy in the BBSome to regulate the degradative sorting of ciliary
646 sensory receptors. *Sci. Rep.* 5:11855. doi:10.1038/srep11855.

647 Yau, R., and M. Rape. 2016. The increasing complexity of the ubiquitin code. *Nat. Cell Biol.*
648 18:579–586. doi:10.1038/ncb3358.

649 Ye, F., A.R. Nager, and M.V. Nachury. 2018. BBSome trains remove activated GPCRs from
650 cilia by enabling passage through the transition zone. *J. Cell Biol.* 217:1847–1868.
651 doi:10.1083/jcb.201709041.

652 Yue, S., L.-Y. Tang, Y. Tang, Y. Tang, Q.-H. Shen, J. Ding, Y. Chen, Z. Zhang, T.-T. Yu, Y.E.
653 Zhang, and S.Y. Cheng. 2014. Requirement of Smurf-mediated endocytosis of Patched1
654 in sonic hedgehog signal reception. *eLife.* 3:128. doi:10.7554/eLife.02555.

655 Zhang, Q., D. Nishimura, S. Seo, T. Vogel, D.A. Morgan, C. Searby, K. Bugge, E.M. Stone, K.
656 Rahmouni, and V.C. Sheffield. 2011. Bardet-Biedl syndrome 3 (Bbs3) knockout mouse

model reveals common BBS-associated phenotypes and Bbs3 unique phenotypes. *Proc Natl Acad Sci U A*. 108:20678–20683. doi:10.1073/pnas.1113220108.

661 **ACKNOWLEDGMENTS**

662 We thank Drs. Kirk Mykytyn, Val Sheffield, Alice Ting, and Mark Scott for the gifts of cDNAs;
663 Kathryn Anderson, Vishva Dixit, and Felice Dunn for the gifts of antibodies; Val Sheffield for
664 the gift of the *Bbs4*$^{-/-}$ mice, George B. Witman and the Chlamydomonas Resource Center for the
665 gift of *Chlamydomonas* strains; Yien-Ming Kuo for help with cryosections of mouse retina and core
666 support; Dhivya Kumar and Tyler Picariello for the assistance with *Chlamydomonas* cultures;
667 Nicholas Morante and Jeremy Reiter for providing *Bbs4*$^{-/-}$ mouse eyes; Fan Ye for generating
668 some of the cell lines used in the study; Irene Ojeda Naharros for help with single cilia tracking,
669 the Nachury and von Zastrow labs for helpful discussions and the Ogden and Caspary labs for
670 comments on the preprint. This work was funded by NIGMS (R01-GM089933, M.V.N.). This
671 work was made possible, in part, by NEI EY002162 - Core Grant for Vision Research and by
672 the Research to Prevent Blindness Unrestricted Grant (M.V.N.). Authors contributions: SRS
673 conducted all experimental work except for the experiments in Figure 5 which were conducted
674 by ARN. MVN supervised research. SRS and MVN wrote the manuscript.
675

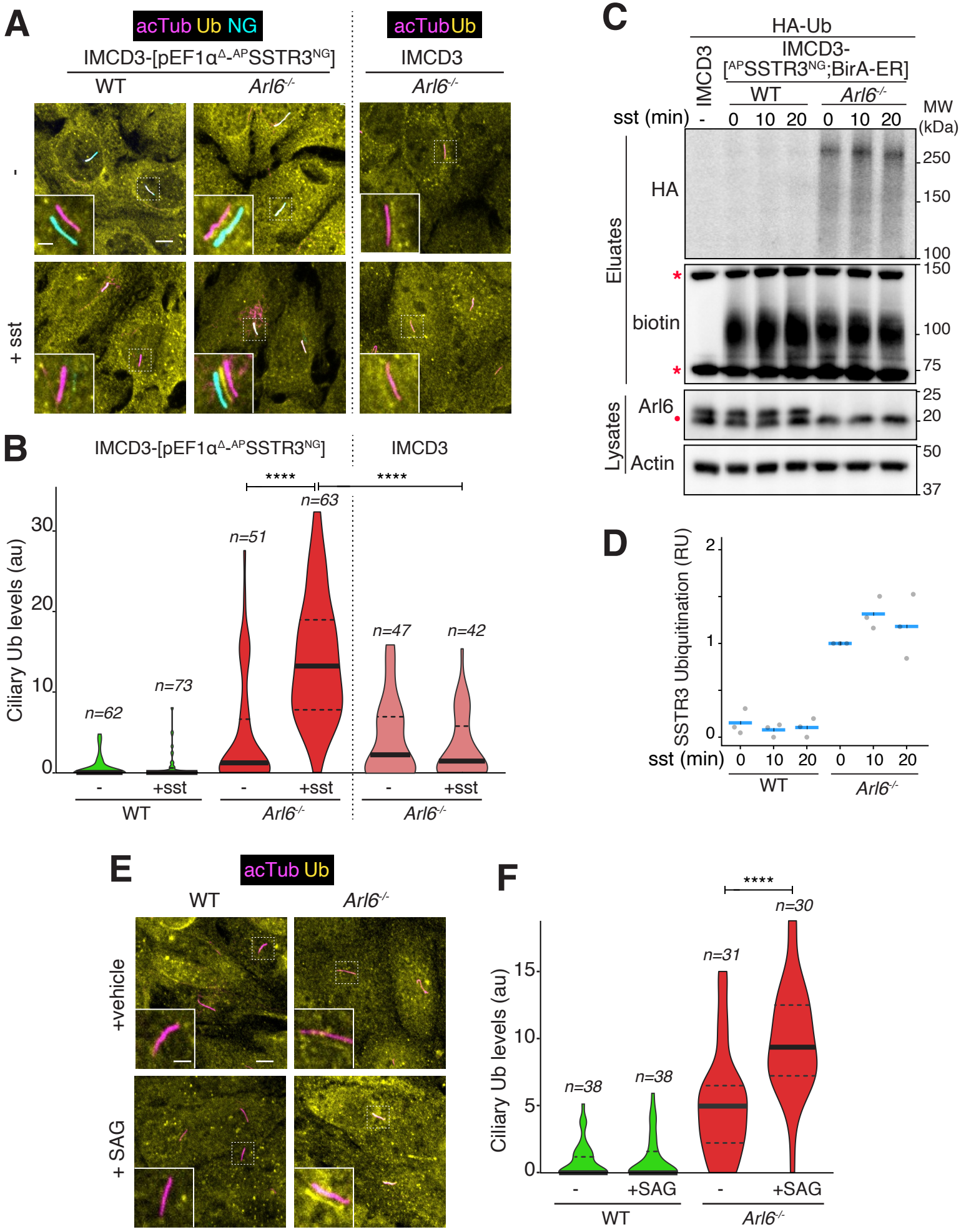
A
acTub Ub NG
IMCD3-[pEF1α$^{\Delta}$-$^{AP}$SSTR3$^{NG}$]
WT
Arl6-/-
acTub Ub
IMCD3
Arl6-/-
-
+ sst
B
IMCD3-[pEF1α$^{\Delta}$-$^{AP}$SSTR3$^{NG}$]
IMCD3
Ciliary Ub levels (au)
****
****
n=62
n=73
n=51
n=63
n=47
n=42
-
+sst
-
+sst
-
+sst
WT
Arl6-/-
Arl6-/-
C
HA-Ub
IMCD3
IMCD3-[$^{AP}$SSTR3$^{NG}$;BirA-ER]
WT
Arl6-/-
sst (min)
-
0
10
20
0
10
20
MW (kDa)
Eluates
HA
biotin
Lysates
Arl6
Actin
250
150
100
150
100
75
25
20
50
37
D
SSTR3 Ubiquitination (RU)
sst (min)
0
10
20
0
10
20
WT
Arl6-/-
E
acTub Ub
WT
Arl6-/-
+vehicle
+ SAG
F
****
Ciliary Ub levels (au)
n=38
n=38
n=31
n=30
-
+SAG
-
+SAG
WT
Arl6-/-

**Figure 1**

676 **Figure 1. Ubiquitinated signaling receptors accumulate inside cilia of *Arl6*$^{-/-}$ cells**
677 **A.** SSTR3 fused to the fluorescent protein mNeonGreen (NG) at its intracellular C-terminus and
678 a biotinylation Acceptor Peptide (AP) tag at its extracellular N-terminus was expressed under the
679 control of an attenuated EF1α promoter (pEF1α$^{\Delta}$) in wild type (WT) and *Arl6*$^{-/-}$ IMCD3 cells.
680 Cells were treated with or without somatostatin-14 (sst) for 2 h, then fixed and stained for
681 acetylated tubulin (acTub, magenta) and ubiquitin (Ub, yellow). $^{AP}$SSTR3$^{NG}$ (cyan) was imaged
682 through the intrinsic fluorescence of NG. Channels are shifted in the insets to facilitate
683 visualization of overlapping ciliary signals. Scale bar: 5μm (main panel), 2μm (inset). In WT cells,
684 the ciliary SSTR3 signal decreases over the experimental time course. In *Arl6*$^{-/-}$ cells, SSTR3 fails
685 to exit cilia and an increase in the ciliary Ub level is detected. As a control, *Arl6*$^{-/-}$ cells that did
686 not express SSTR3-NG were tested; no increase in ciliary Ub levels was observed upon addition
687 of sst. **B.** The fluorescence intensity of the Ub channel in the cilium was measured in each
688 condition and the data are represented as violin plots. The thick bar indicates the median and the
689 dotted lines the first and third quartiles. An 11-fold increase in ciliary Ub signal is observed upon
690 addition of sst to SSTR3-expressing cells. Asterisks indicate ANOVA significance value. ****, p=
691 <0.0001. **C.** WT or *Arl6*$^{-/-}$ IMCD3 cells stably expressing $^{AP}$SSTR3$^{NG}$ and the biotin ligase BirA
692 targeted to the ER lumen (BirA-ER ) were transiently transfected with HA-tagged ubiquitin (HA-
693 Ub). 10 μM biotin was added to cells 24 h post transfection for maximal biotinylation of
694 $^{AP}$SSTR3$^{NG}$ and, after another 18 h, cells were treated with sst (10μM) for indicated times. Cells
695 were lysed under denaturing conditions and biotinylated SSTR3 was captured on streptavidin
696 resin. Eluates were probed for HA via immunoblotting and for biotin via streptavidin-HRP. Two
697 major biotinylated proteins endogenous to cells are marked by asterisks. Whole cell lysates were
698 probed for Arl6 and, as a loading control, actin. A non-specific band cross-reacting with the anti-
699 Arl6 antibody is marked with a dot. **D.** Quantitation of SSTR3 ubiquitination. The signals of
700 HA-Ub conjugated to SSTR3 in the streptavidin eluates were measured. The experiment shown
701 in **C** was repeated three times and for each experiment, Ub-SSTR3 signals were normalized to
702 the value in *Arl6*$^{-/-}$ cells at t = 0 of sst stimulation and plotted as grey circles. The horizontal blue
703 lines represent mean values. **E.** IMCD3 cells of the indicated genotypes were treated with the

704 Smoothened agonist SAG or the vehicle DMSO for 2h. Cells were then fixed and stained for
705 acTub and Ub. Channels are shifted in the insets to facilitate visualization of overlapping ciliary
706 signals. Scale bar 5μm (main panel), 2μm (inset). Activation of Hh signaling promotes a
707 detectable increase in ciliary Ub levels only in *Arl6*$^{-/-}$ cells. **F.** Violin plots of the fluorescence
708 intensity of the Ub channel in the cilium in each condition are shown. Asterisks indicate
709 ANOVA significance value. ****, p= <0.0001.
710
711

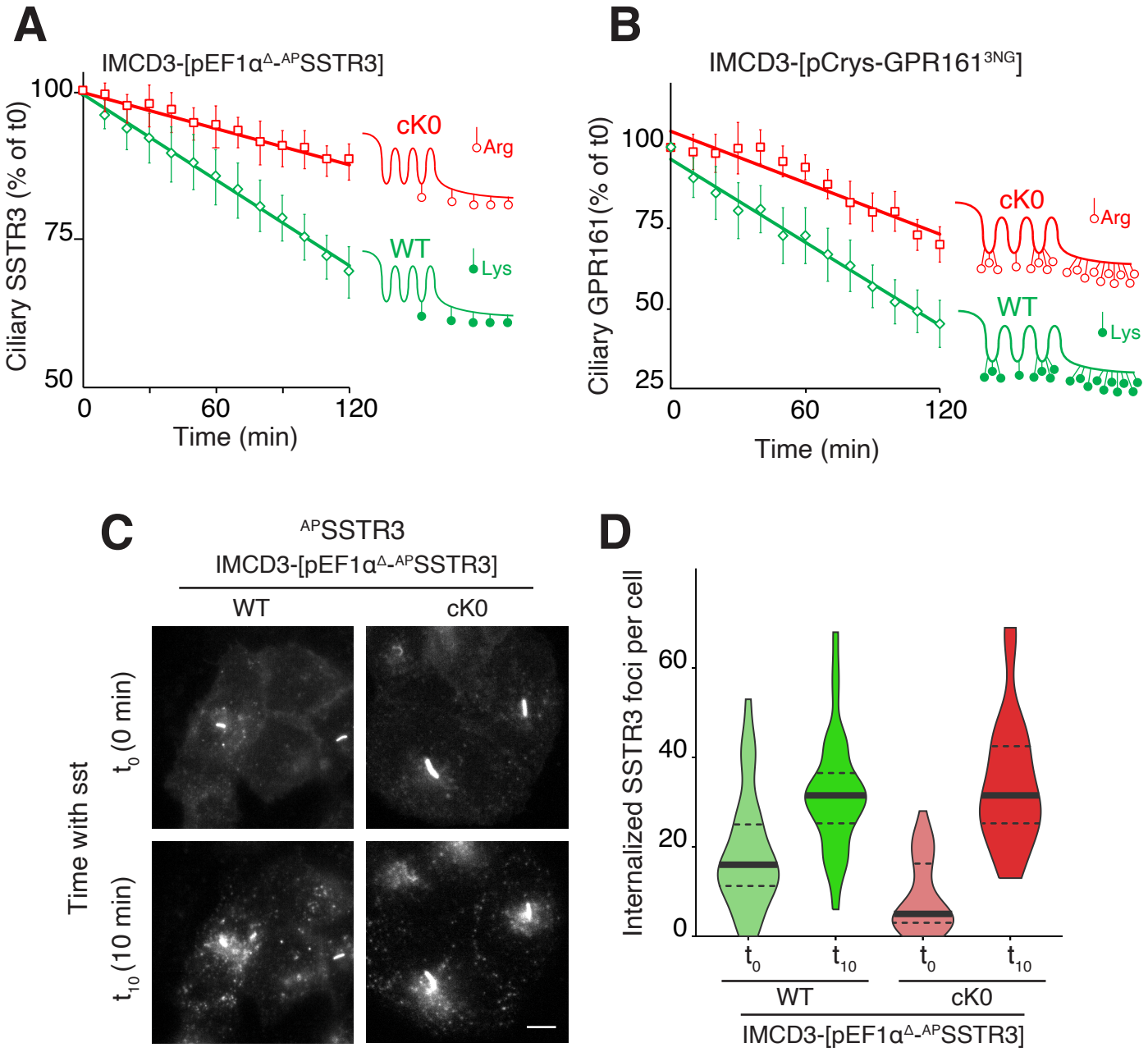
A
IMCD3-[pEF1α$^{\Delta}$-$^{AP}$SSTR3]
Ciliary SSTR3 (% of t0)
100
75
50
0
60
120
Time (min)
cK0
Arg
WT
Lys
B
IMCD3-[pCrys-GPR161$^{3NG}$]
Ciliary GPR161 (% of t0)
100
75
50
25
0
60
120
Time (min)
cK0
Arg
WT
Lys
C
$^{AP}$SSTR3
IMCD3-[pEF1α$^{\Delta}$-$^{AP}$SSTR3]
WT
cK0
Time with sst
$t_0$ (0 min)
$t_{10}$ (10 min)
D
Internalized SSTR3 foci per cell
60
40
20
0
$t_0$
$t_{10}$
$t_0$
$t_{10}$
WT
cK0
IMCD3-[pEF1α$^{\Delta}$-$^{AP}$SSTR3]

**Figure 2**

712 **Figure 2. Ubiquitination of ciliary GPCRs is required for signal-dependent exit but**
713 **not for endocytosis.**
714 **A.** IMCD3-[pEF1α$^{\Delta}$-$^{AP}$SSTR3] cells stably expressed the ER-localized biotin ligase BirA to
715 enables the biotinlylation of $^{AP}$SSTR3. SSTR3 was either the wild-type allele (WT) or a variant
716 where all five cytoplasm-facing lysine residues (listed in Methods) were mutated to arginine (cK0).
717 Ciliary $^{AP}$SSTR3 was pulse-labeled by addition of Alexa647-conjugated mSA (mSA647) to the
718 medium for 5-10 min before addition of sst. Far red fluorescence was tracked in individual cilia at
719 10 min capture intervals. For each individual cilia, fluorescence intensities were normalized to
720 the value at t = 0. A comparison of the ciliary levels of SSTR3 at t=0 is shown in **Fig. S2A**. Data
721 were plotted and fitted to a line. Error bars: 95% CI. $N$ =18-22 cilia. **B.** GPR161 fused to three
722 tandem repeats of NG at its C-terminus was expressed under the control of the ultra-weak δ-
723 crystallin promoter (pCrys) in IMCD3 cells. GPR161 was either the wild-type allele (WT) or a
724 variant where all eighteen cytoplasm-facing lysine residues (listed in Methods) where mutated to
725 arginine (cK0). IMCD3-[pCrys-GPR161$^{3NG}$] cells were treated with SAG for 2h. During the
726 course of the experiment, NG fluorescence was tracked in individual cilia at 10 min capture
727 intervals. Fluorescence data were acquired and analyzed as in panel **(A)**. A comparison of the
728 ciliary levels of GPR161 at t=0 is shown in **Fig. S2B**. Error bars: 95% CI. $N$ =10-19 cilia. **C.**
729 IMCD3-[$^{AP}$SSTR3; BirA-ER] cells expressing either WT or cK0 SSTR3 were pulse-labeled by
730 addition of Alexa647-conjugated mSA (mSA647) to the medium for 5 min before addition of sst
731 and were imaged by far red fluorescence immediately after addition of sst ($t_0$) and 10 min later
732 ($t_{10}$). The contrast level was adjusted to reveal plasma membrane-localized and internalized
733 $^{AP}$SSTR3, causing the cilia-localized $^{AP}$SSTR3 signal to reach saturation. Scale bar 5μm. **D.**
734 Internalized $^{AP}$SSTR3 foci were counted immediately after addition of sst ($t_0$) and 10 min later
735 ($t_{10}$), n = 34 cells.

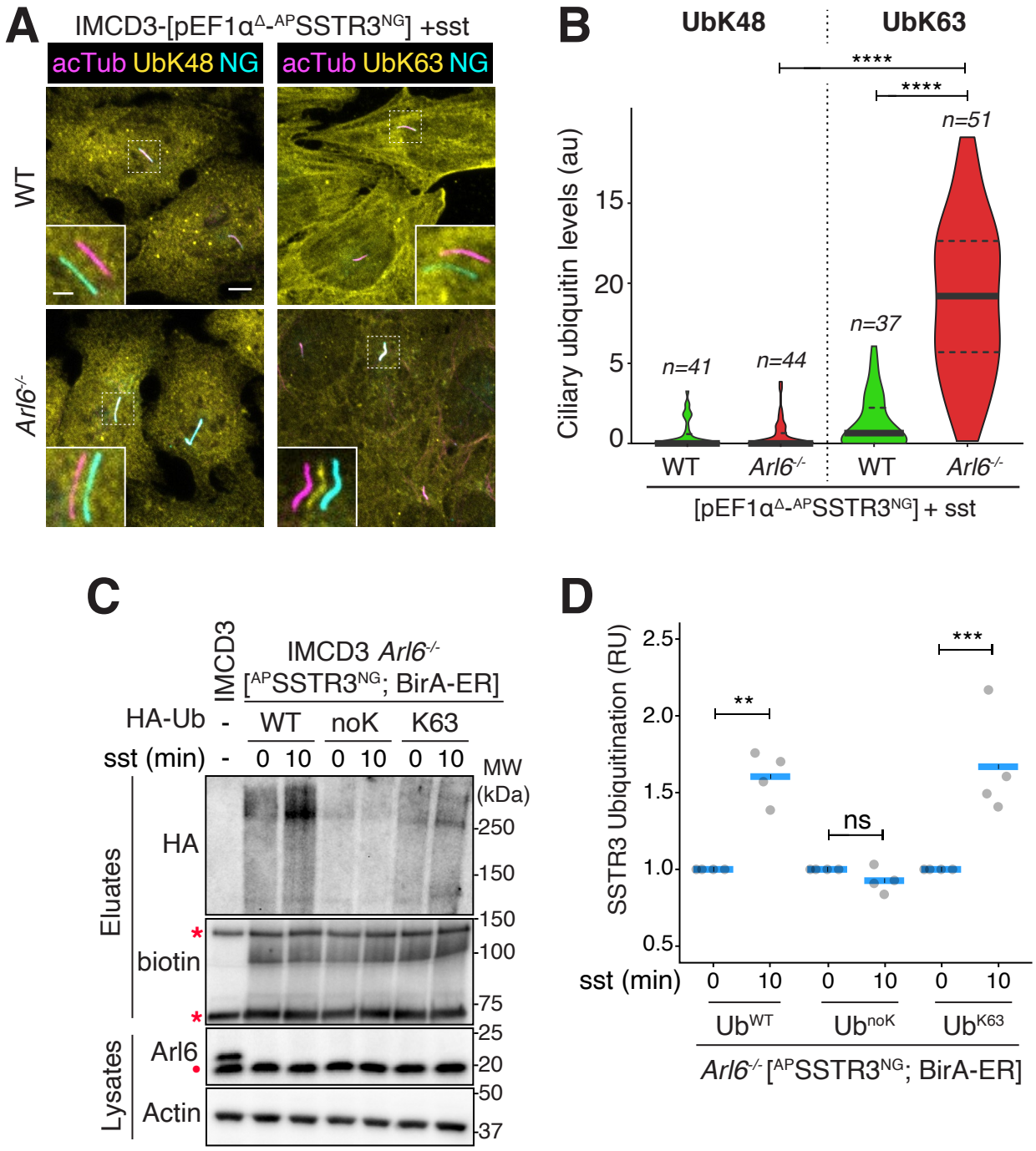
A
IMCD3-[pEF1α$^{\Delta}$-$^{AP}$SSTR3$^{NG}$] +sst
acTub UbK48 NG
acTub UbK63 NG
WT
Arl6$^{-/-}$
B
UbK48
UbK63
****
****
n=51
n=37
n=41
n=44
Ciliary ubiquitin levels (au)
0
5
15
20
WT
Arl6$^{-/-}$
WT
Arl6$^{-/-}$
[pEF1α$^{\Delta}$-$^{AP}$SSTR3$^{NG}$] + sst
C
IMCD3
IMCD3 Arl6$^{-/-}$
[$^{AP}$SSTR3$^{NG}$; BirA-ER]
HA-Ub - WT noK K63
sst (min) - 0 10 0 10 0 10
MW (kDa)
Eluates
HA
biotin
Lysates
Arl6
Actin
250
150
150
100
75
25
20
50
37
D
SSTR3 Ubiquitination (RU)
2.5
2.0
1.5
1.0
0.5
**
ns
***
sst (min) 0 10 0 10 0 10
Ub$^{WT}$
Ub$^{noK}$
Ub$^{K63}$
Arl6$^{-/-}$ [$^{AP}$SSTR3$^{NG}$; BirA-ER]

**Figure 3**

736 **Figure 3. Signal-dependent accumulation of K63-linked ubiquitin chains inside**
737 **cilia of *Bbs* mutant cells.**
738 **A.** IMCD3 cells of the indicated genotypes expressing $^{AP}$SSTR3$^{NG}$ were treated with
739 somatostatin-14 for 2 h. Cells were fixed and stained for AcTub (magenta) and with antibodies
740 specific for the lysine 63 (UbK63) or lysine 48 (UbK48) Ub chain linkages (yellow). SSTR3$^{NG}$
741 (cyan) was imaged through the intrinsic fluorescence of NG. Channels are shifted in the insets to
742 facilitate visualization of overlapping ciliary signals. Scale bar 5µm (main panel), 2µm (inset). **B.**
743 The fluorescence intensity of the UbK48 and UbK63 channels in the cilium are represented as
744 violin plots. A 14-fold increase in ciliary Ub abundance is detected with the K63Ub linkage-
745 specific antibody. Asterisks indicate ANOVA significance value. ****, p= <0.0001. No ciliary
746 signal is detected with the K48Ub linkage-specific antibody. **C.** *Arl6*$^{-/-}$ IMCD3-[$^{AP}$SSTR3; BirA-
747 ER] cells were transfected with the HA-tagged ubiquitin variants WT, noK0 (all seven acceptor
748 lysine residues mutated to arginine) or K63 (where all lysine residues are mutated to arginine
749 except for K63). Biotin was included in the culture medium and cells were treated with sst for 0
750 or 10 min. Cells were lysed under denaturing conditions and biotinylated SSTR3 was captured
751 on streptavidin resin. Eluates were probed for HA via immunoblotting and for biotin via
752 streptavidin-HRP. Two major biotinylated proteins endogenous to cells are marked by asterisks.
753 Whole cell lysates were probed for Arl6 and, as a loading control, actin. A non-specific band
754 cross-reacting with the anti-Arl6 antibody is marked with a dot. WT IMCD3 cells were processed
755 in parallel as a control. **D.** Quantitation of SSTR3 ubiquitination. The signals of HA-Ub
756 conjugated to SSTR3 in the streptavidin eluates were measured. The experiment shown in **C**
757 was repeated four times and for each Ub variant, Ub-SSTR3 signals were normalized to the
758 value at t = 0 of sst stimulation and plotted as grey circles. The horizontal blue lines represent
759 mean values. Asterisks indicate ANOVA significance value. *** p =< 0.001; ** p=<0.01.
760

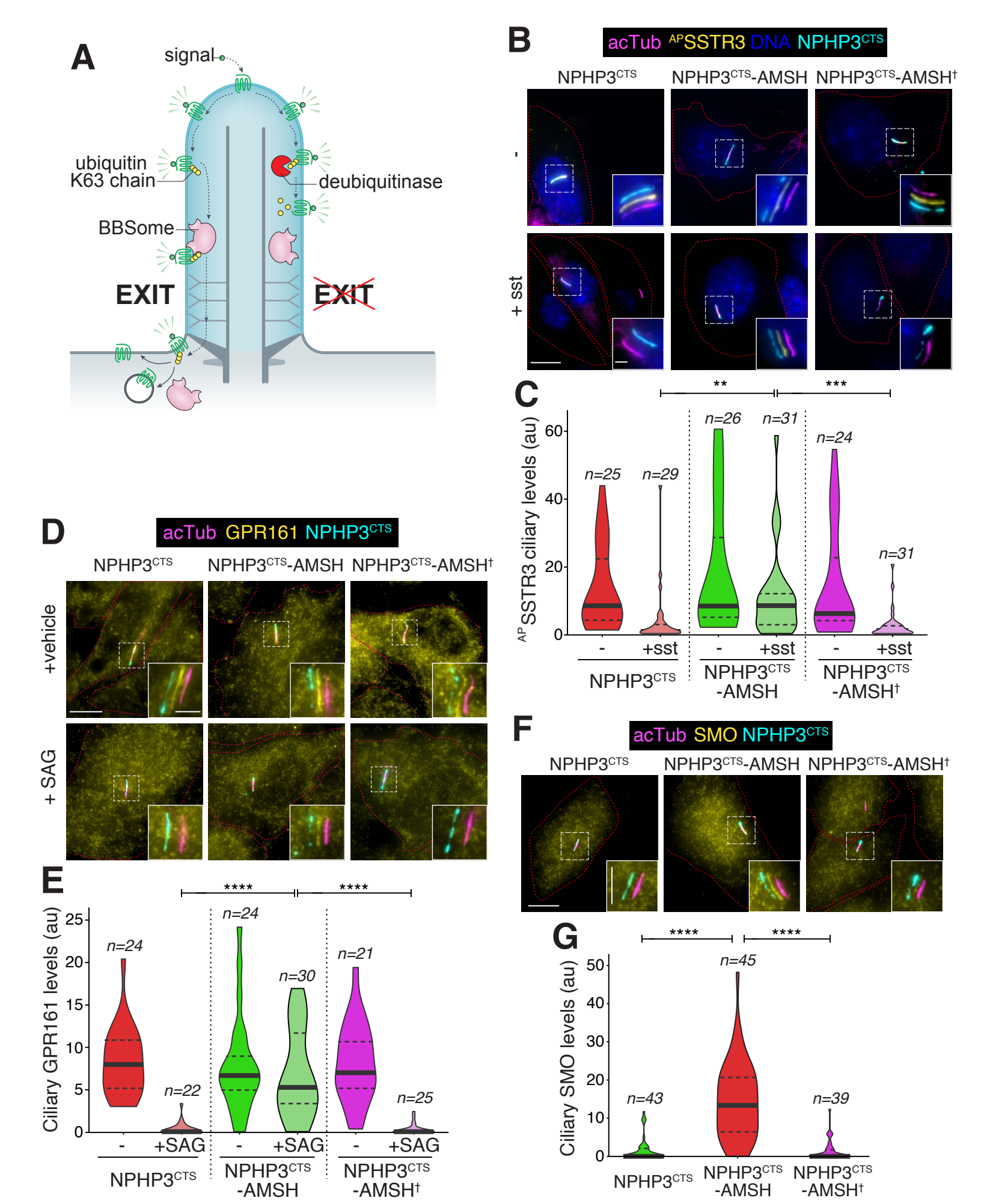
A
signal
ubiquitin
K63 chain
deubiquitinase
BBSome
EXIT
EXIT
B
acTub APSSTR3 DNA NPHP3CTS
NPHP3CTS
NPHP3CTS-AMSH
NPHP3CTS-AMSH†
-
+ sst
C
APSSTR3 ciliary levels (au)
n=25
n=29
n=26
n=31
n=24
n=31
**
***
-
+sst
NPHP3CTS
NPHP3CTS -AMSH
NPHP3CTS -AMSH†
D
acTub GPR161 NPHP3CTS
NPHP3CTS
NPHP3CTS-AMSH
NPHP3CTS-AMSH†
+vehicle
+ SAG
E
Ciliary GPR161 levels (au)
n=24
n=22
n=24
n=30
n=21
n=25
****
****
-
+SAG
NPHP3CTS
NPHP3CTS -AMSH
NPHP3CTS -AMSH†
F
acTub SMO NPHP3CTS
NPHP3CTS
NPHP3CTS-AMSH
NPHP3CTS-AMSH†
G
Ciliary SMO levels (au)
n=43
n=45
n=39
****
****
NPHP3CTS
NPHP3CTS -AMSH
NPHP3CTS -AMSH†

**Figure 4**

761 **Figure 4. Ciliary K63-linked ubiquitin chains are required for GPCR exit from**
762 **cilia.**
763 **A.** Diagram of the working model and the experimental strategy. **B.** IMCD3-[pEF1α$^{\Delta}$-
764 $^{AP}$SSTR3; pEF1α-BirA•ER] were transfected with plasmids expressing the ciliary targeting signal
765 (CTS) of NPHP3 fused to GFP only (left panels), to GFP and the catalytic domain of the K63-
766 specific deubiquitinase AMSH (middle panels), or to GFP and the catalytically inactive E280A
767 variant of AMSH catalytic domain (AMSH$^{\dagger}$, right panels). Ciliary $^{AP}$SSTR3 was pulse-labeled
768 with mSA647 for 5-10 min and cells were then treated with or without sst for 2h, before fixation
769 and staining for acetylated tubulin (acTub, magenta) and DNA (blue). The NPHP3$^{CTS}$ fusions
770 were visualized through the intrinsic fluorescence of GFP (cyan) and $^{AP}$SSTR3 was visualized via
771 mSA647 (yellow). Channels are shifted in the insets to facilitate visualization of overlapping
772 ciliary signals. Scale bar 5μm (main panel), 2μm (inset). **C.** The fluorescence intensities of ciliary
773 $^{mSA647\text{-}AP}$SSTR3 are represented as violin plots. Asterisks indicate Kruskal-Wallis test significance
774 values. ***, p= <0.001; **, p= <0.01. Addition of sst triggers the exit of SSTR3 from cilia in cells
775 transfected with the controls NPHP3$^{CTS}$ and NPHP3$^{CTS}$-AMSH$^{\dagger}$ but NPHP3$^{CTS}$-AMSH blocks
776 ciliary exit of SSTR3. **D.** RPE1-hTERT (RPE) cells transfected with the indicated constructs
777 were treated with SAG or vehicle (DMSO) for 2h, then fixed and stained for acetylated tubulin
778 (magenta) and GPR161 (yellow). The NPHP3$^{CTS}$ fusions were visualized through the intrinsic
779 fluorescence of GFP (cyan). Channels are shifted in the insets to facilitate visualization of
780 overlapping ciliary signals. Scale bar 5μm (main panel), 2μm (inset). **E.** The fluorescence
781 intensities of ciliary GPR161 are represented as violin plots. Asterisks indicate ANOVA
782 significance value. ****, p= <0.0001. NPHP3$^{CTS}$-AMSH specifically blocks the SAG-dependent
783 exit of GPR161 from cilia. **F.** IMCD3 cells transfected with the indicated constructs were fixed
784 and stained for acetylated tubulin (magenta) and SMO (yellow). The NPHP3$^{CTS}$ fusions were
785 visualized through the intrinsic fluorescence of GFP (cyan). Channels are shifted in the insets to
786 facilitate visualization of overlapping ciliary signals. **G.** The fluorescence intensities of ciliary
787 SMO are represented as violin plots. Asterisks indicate ANOVA significance value. ****, p=

788 <0.0001. NPHP3$^{CTS}$-AMSH specifically blocks the constitutive exit of SMO from cilia and
789 promotes accumulation of SMO in cilia in the absence of pathway activation.

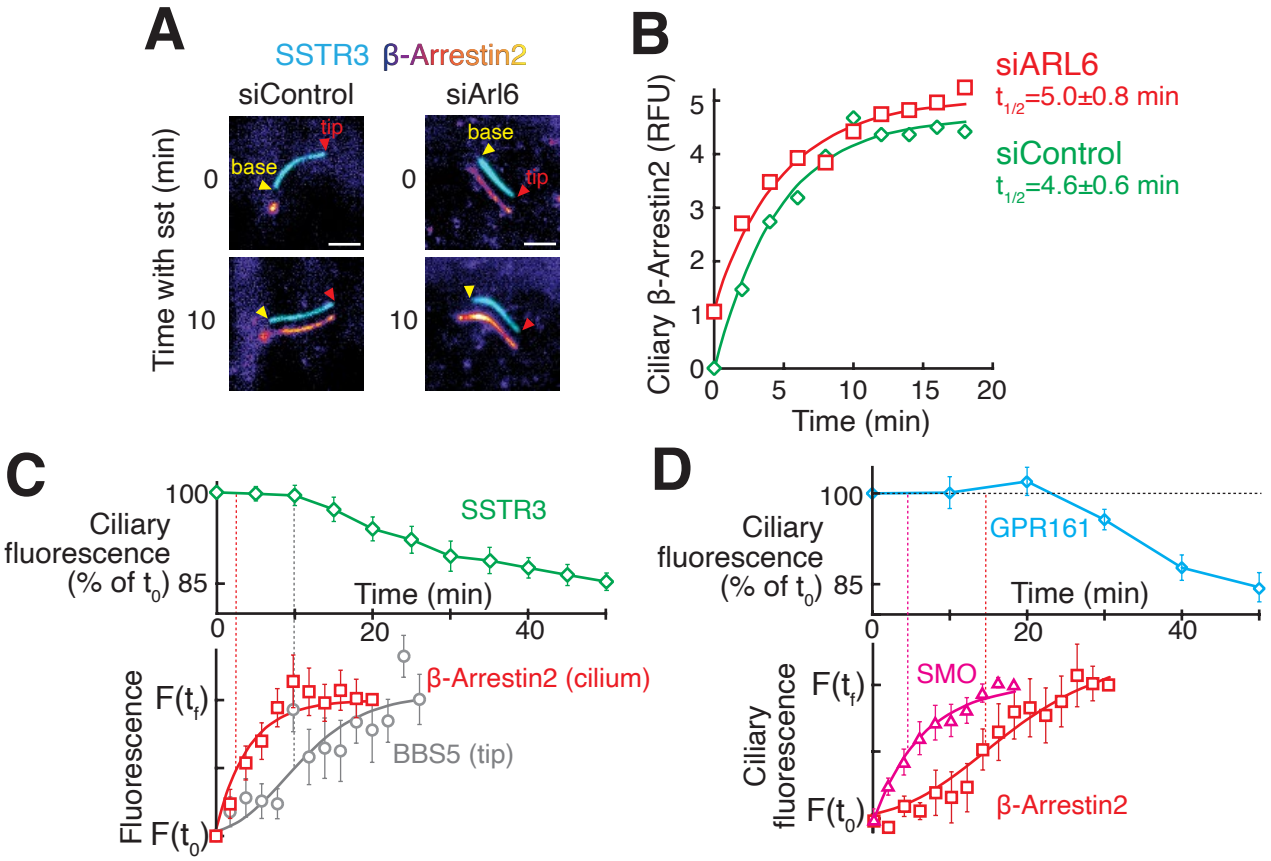
A
SSTR3 β-Arrestin2
siControl
siArl6
Time with sst (min)
0
10
tip
base
B
siARL6
$t_{1/2}$=5.0±0.8 min
siControl
$t_{1/2}$=4.6±0.6 min
Ciliary β-Arrestin2 (RFU)
Time (min)
C
Ciliary fluorescence (% of $t_0$)
SSTR3
Time (min)
β-Arrestin2 (cilium)
BBS5 (tip)
Fluorescence
$F(t_f)$
$F(t_0)$
D
GPR161
SMO
β-Arrestin2
Ciliary fluorescence

**Figure 5**

790 **Figure 5. β-arrestin 2 is recruited to cilia upon activation of SSTR3 or GPR161.**

791 **A.** β-Arrestin2 is rapidly recruited to cilia upon activation of SSTR3. siRNA-treated IMCD3-
792 [$^{AP}$SSTR3, β-Arrestin2$^{GFP}$] cells were pulse-labeled with mSA647 before addition of sst.
793 Channels are shifted to facilitate visualization of overlapping ciliary signals. As shown previously
794 (Shankar et al., 2010), β-Arrestin2 is at the basal body in unstimulated cells. Scale bar: 2 μm. **B.**
795 Kinetics of β-Arrestin2$^{GFP}$ recruitment to cilia upon sst stimulation in control- and ARL6-
796 depleted IMCD3-[$^{AP}$SSTR3, β-Arrestin2$^{GFP}$] cells. Data were fit to a simple exponential. (n=10
797 cilia). **C-D.** Kinetics of early trafficking events for retrieval of SSTR3 (**C**) and GPR161 (**D**). The
798 top panels show removal of stably expressed $^{AP}$SSTR3$^{NG}$ or $^{AP}$GPR161$^{NG3}$ following addition of
799 sst (**C**) or SAG (**D**). The bottom panels show the kinetics of β-Arrestin2$^{GFP}$ entry (**C-D**),
800 $^{AP}$Smoothened$^{NG}$ entry (**D**), and $^{NG3}$BBS5 tip accumulation (**C**) measured in IMCD3 cells stably
801 expressing the indicated proteins. Fluorescence values are normalized to the initial ($t_0$) and final
802 ($t_f$) values. Error bars: SEM. (n=6-11 cilia).
803

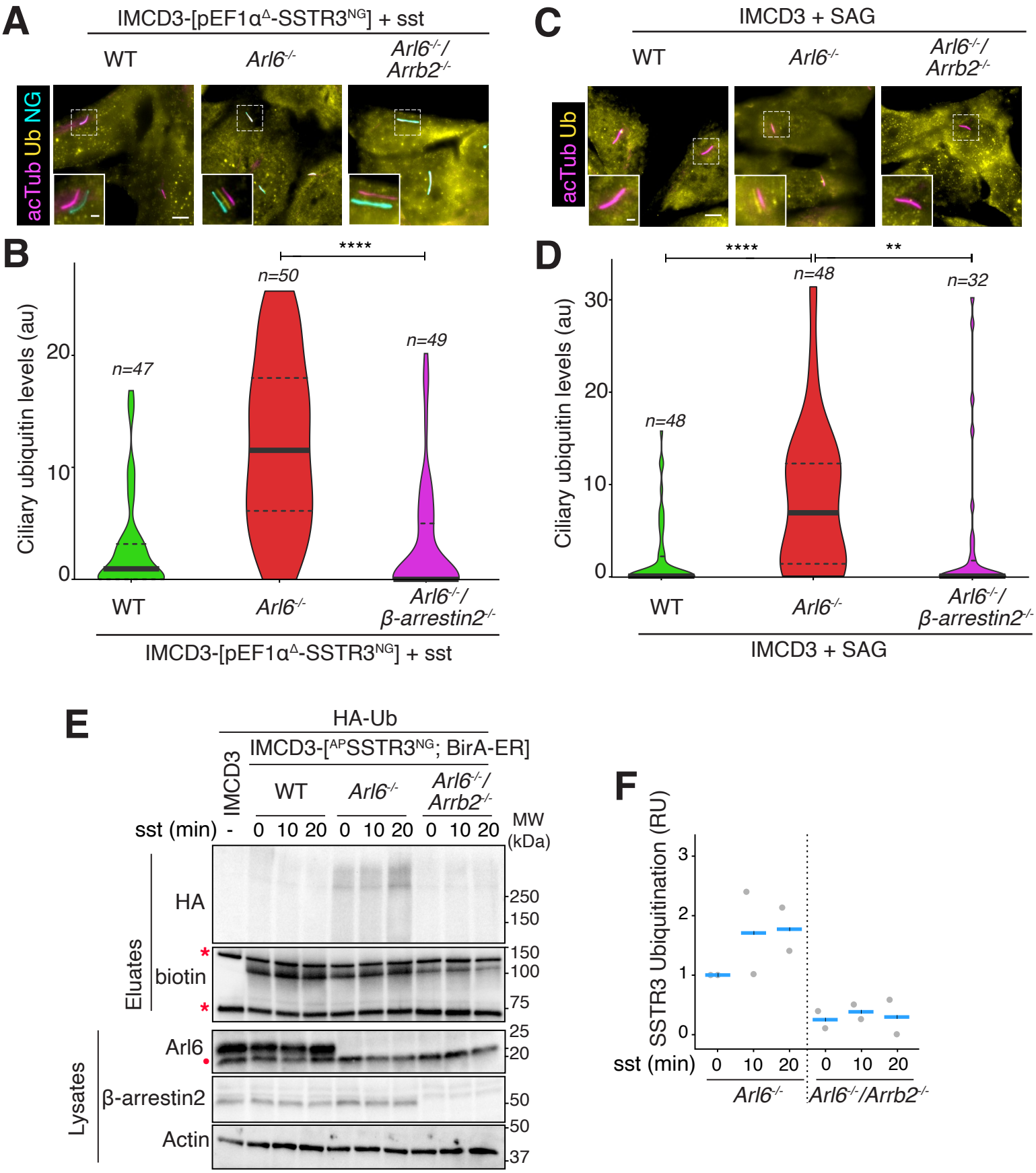
A
IMCD3-[pEF1α$^{\Delta}$-SSTR3$^{NG}$] + sst
WT
Arl6$^{-/-}$
Arl6$^{-/-}$/ Arrb2$^{-/-}$
acTub Ub NG
C
IMCD3 + SAG
WT
Arl6$^{-/-}$
Arl6$^{-/-}$/ Arrb2$^{-/-}$
acTub Ub
B
Ciliary ubiquitin levels (au)
****
n=47
n=50
n=49
WT
Arl6$^{-/-}$
Arl6$^{-/-}$/ β-arrestin2$^{-/-}$
IMCD3-[pEF1α$^{\Delta}$-SSTR3$^{NG}$] + sst
D
Ciliary ubiquitin levels (au)
****
**
n=48
n=48
n=32
WT
Arl6$^{-/-}$
Arl6$^{-/-}$/ β-arrestin2$^{-/-}$
IMCD3 + SAG
E
HA-Ub
IMCD3
IMCD3-[$^{AP}$SSTR3$^{NG}$; BirA-ER]
WT
Arl6$^{-/-}$
Arl6$^{-/-}$/ Arrb2$^{-/-}$
sst (min) - 0 10 20 0 10 20 0 10 20
MW (kDa)
Eluates
HA
biotin
Lysates
Arl6
β-arrestin2
Actin
250
150
150
100
75
25
20
50
50
37
F
SSTR3 Ubiquitination (RU)
sst (min) 0 10 20 0 10 20
Arl6$^{-/-}$
Arl6$^{-/-}$/Arrb2$^{-/-}$

**Figure 6**

804 **Figure 6. β-arrestin 2 directs the signal-dependent ubiquitination of ciliary**
805 **GPCRs.**
806 **A.** IMCD3-[pEF1α$^{\Delta}$-$^{AP}$SSTR3$^{NG}$] cells of the indicated genotypes were treated with sst for 2h
807 before fixation and staining for acetylated tubulin (acTub, magenta) and ubiquitin (Ub, yellow).
808 SSTR3$^{NG}$ was visualized through the intrinsic fluorescence of NG (cyan). Channels are shifted in
809 the insets to facilitate visualization of overlapping ciliary signals. SSTR3 exit is blocked in *Arl6*$^{-/-}$
810 cells regardless of the *β-Arrestin2* genotype but the ciliary Ub signal is only evident when β-
811 Arrestin2 function is intact. Scale bar: 5μm (main panel), 1μm (inset). **B.** Violin plots
812 representing the ciliary levels of Ub under the indicated conditions. Asterisks indicate ANOVA
813 significance value. ****, p= <0.0001. **C.** IMCD3 WT, knockout for *Arl6* only and double
814 knockout for *Arl6* and the β-Arrestin2 gene *Arrb2* were treated with SAG for 2h before fixation
815 and staining for acetylated tubulin (acTub, magenta) and ubiquitin (Ub, yellow). Channels are
816 shifted in the insets to facilitate visualization of overlapping ciliary signals. Scale bar: 5μm (main
817 panel), 1μm (inset). **D.** Violin plots representing the ciliary Ub levels. Asterisks indicate ANOVA
818 significance value. ****, p= <0.0001; **, p= <0.01. The appearance of a Ub signal in cilia in
819 *Arl6*$^{-/-}$ cells depends on β-Arrestin2. **E.** IMCD3-[$^{AP}$SSTR3; BirA-ER] cells of the indicated
820 genotypes stably expressing $^{AP}$SSTR3$^{NG}$ and BirA-ER were transfected with HA-Ub, biotin was
821 added to the medium and cells were treated with sst for indicated times. Biotinylated SSTR3 was
822 captured from cell lysates under denaturing conditions on streptavidin resin. Eluates were probed
823 for HA via immunoblotting and for biotin via streptavidin-HRP. Two major biotinylated
824 proteins endogenous to cells are marked by asterisks. Whole cell lysates were probed for Arl6, β-
825 Arrestin2 to verify genotypes and, as a loading control, actin. A non-specific band cross-reacting
826 with the anti-Arl6 antibody is marked with a dot. WT IMCD3 cells were processed in parallel as
827 a control. **F.** Quantitation of SSTR3 ubiquitination. The signals of HA-Ub conjugated to
828 SSTR3 in the streptavidin eluates were measured. The experiment shown in **E** was repeated
829 twice and for each experiment, Ub-SSTR3 signals were normalized to the value in *Arl6*$^{-/-}$ cells at
830 t = 0 of sst stimulation and plotted as grey circles. The horizontal blue lines represent mean
831 values.

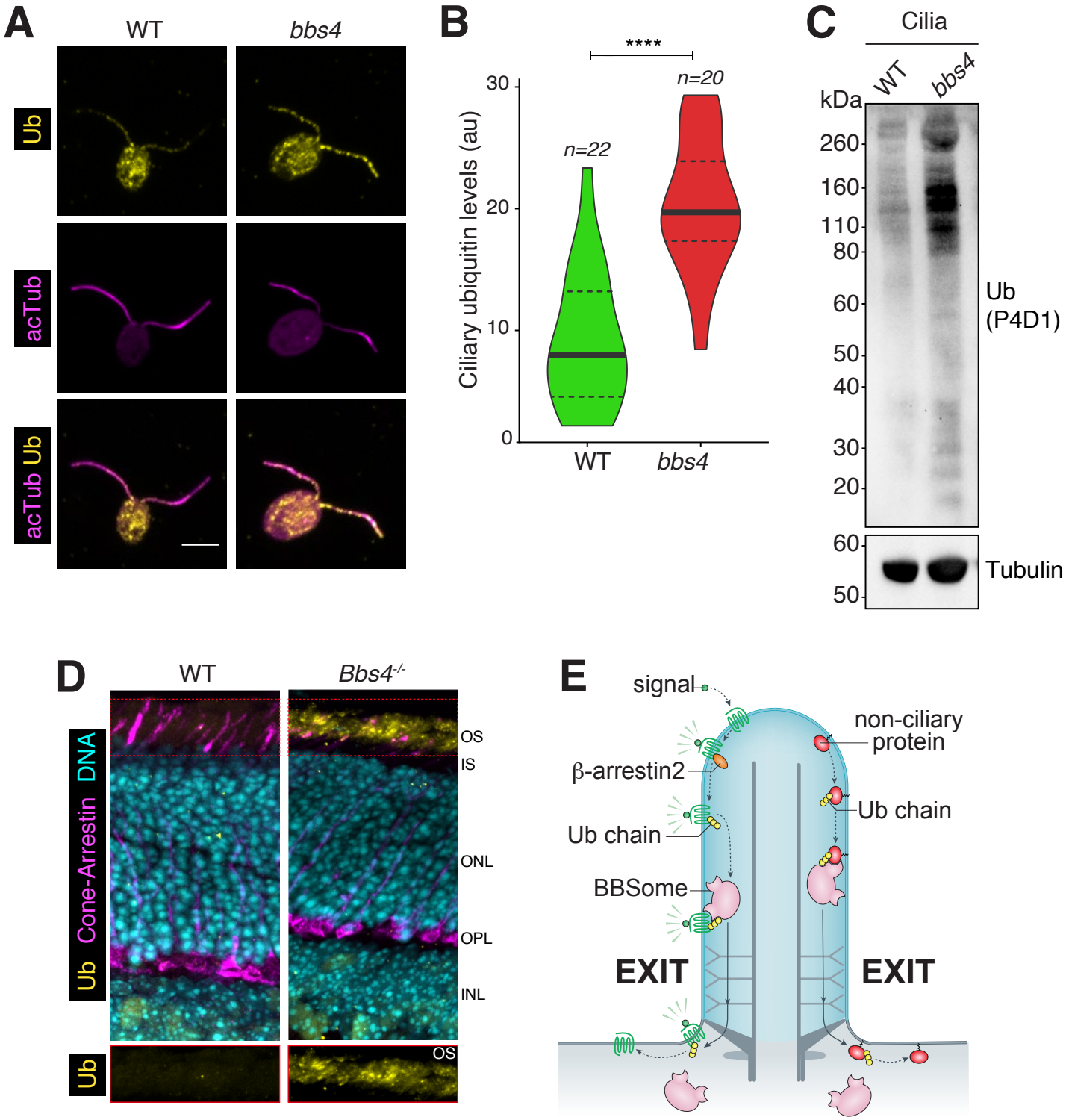
A
WT
bbs4
Ub
acTub
acTub Ub
B
****
n=22
n=20
Ciliary ubiquitin levels (au)
30
20
10
0
WT
bbs4
C
Cilia
WT
bbs4
kDa
260
160
110
80
60
50
40
30
20
Ub
(P4D1)
60
50
Tubulin
D
WT
Bbs4-/-
Ub Cone-Arrestin DNA
OS
IS
ONL
OPL
INL
Ub
OS
E
signal
non-ciliary
protein
β-arrestin2
Ub chain
Ub chain
BBSome
EXIT
EXIT

**Figure 7**

832 **Figure 7. Accumulation of ubiquitinated proteins in cilia of *Chlamydomonas* cells**
833 **and mammalian photoreceptors.**
834 **A.** *Chlamydomonas* cells of the indicated genotypes were fixed and stained for acetylated tubulin
835 (acTub, magenta) and ubiquitin (Ub, yellow). Scale bar: 5 µm. A weak ubiquitin signal detected
836 in WT cells is increased in *bbs4* mutant cells. **B.** Violin plots of the ciliary Ub levels in WT and
837 *bbs4 Chlamydomonas* cells. Asterisks indicate Mann-Whitney test significance values. ****, p=
838 <0.0001. The ciliary levels of Ub are increased more than 2-fold in *bbs4* cells as compared to
839 WT. **C.** Cilia purified from WT and *bbs4* cells via deciliation with dibucaine and differential
840 centrifugation were solubilized, and the protein contents resolved by SDS-PAGE. Immunoblots
841 for Ub (using the P4D1 antibody) and tubulin are shown. A rise in ubiquitin conjugates is
842 observed in *bbs4 Chlamydomonas* cells compared to WT. **D.** Mouse retina were fixed, embedded
843 and sectioned before staining for ubiquitin (Ub, yellow, lower panel), cone arrestin (magenta, a
844 marker of the photoreceptor outer segment layer) and DNA (cyan). OS: outer segment; IS: inner
845 segment; ONL: outer nuclear layer; OPL: outer plexiform layer; INL: inner nuclear layer. Scale
846 bar: 10µm. **E.** Model for the role of ubiquitin chains in selecting cargoes for signal-dependent
847 and constitutive exit via BBSome-mediated transport.
848

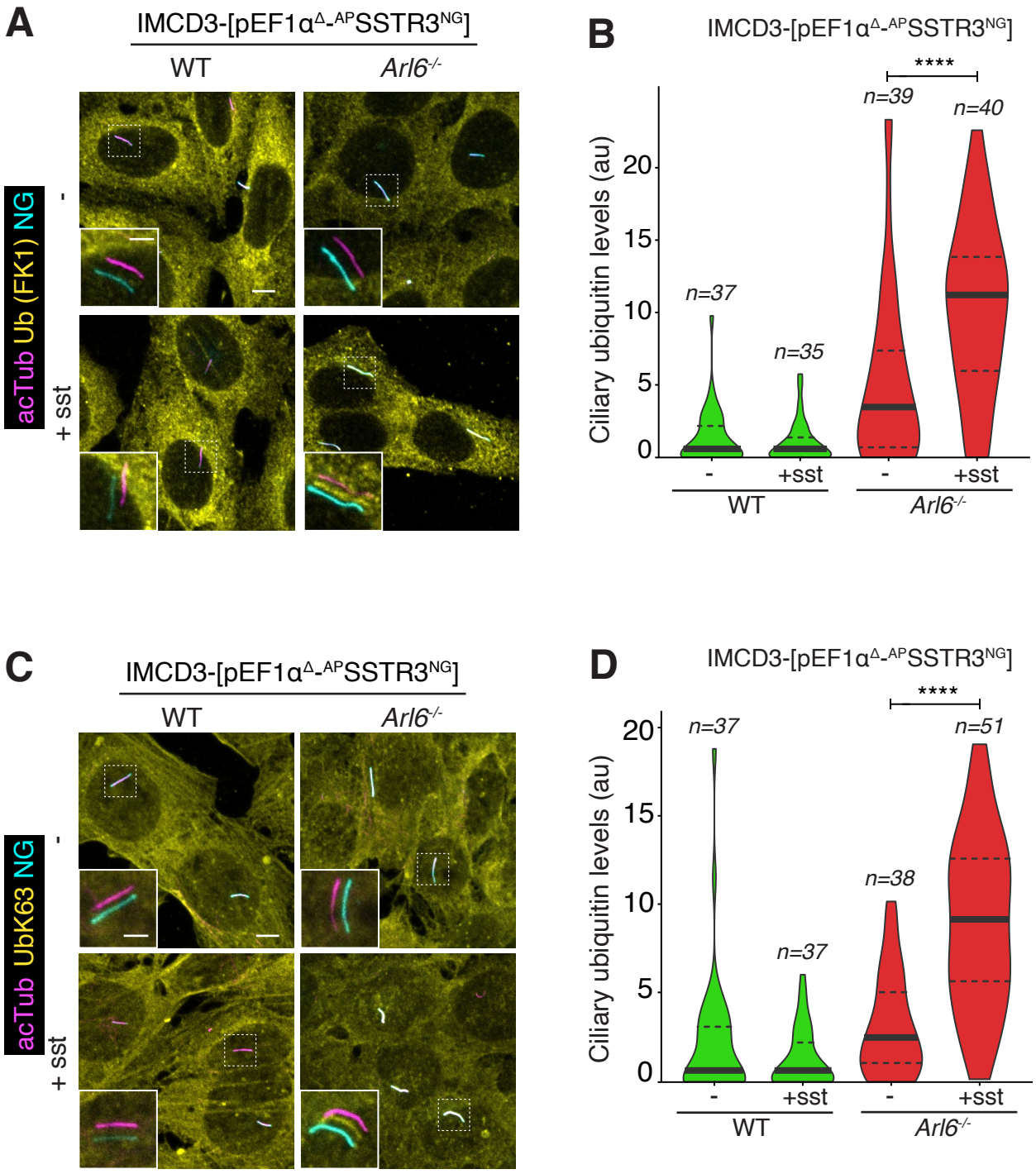


**Supplementary Figure 1**

849 **Figure S1. Signal-dependent ubiquitination of ciliary GPCRs**

850 **A.** IMCD3 cells of the indicated genotypes expressing $^{AP}$SSTR3$^{NG}$ were treated with
851 somatostatin (sst) for 2 h. Cells were fixed and stained for ubiquitin with the FK1 monoclonal
852 antibody (Ub (FK1), yellow) and acetylated tubulin (acTub, magenta). $^{AP}$SSTR3$^{NG}$ (cyan) was
853 imaged through the intrinsic fluorescence of NG. Channels are shifted in the insets to facilitate
854 visualization of overlapping ciliary signals. Scale bar: 5µm (main panel), 2µm (inset). **B.** Violin
855 plots of the fluorescence intensity of the Ub channel in the cilium in each condition are shown. A
856 3-fold increase in ciliary Ub signal is observed upon addition of sst to SSTR3-expressing cells.
857 Asterisks indicate ANOVA significance value. ****, p= <0.0001. **C.** IMCD3 cells of the
858 indicated genotypes expressing $^{AP}$SSTR3$^{NG}$ were treated with sst for 2 h. Cells were fixed and
859 stained for AcTub (magenta) and UbK63 (yellow). $^{AP}$SSTR3$^{NG}$ (cyan) was imaged through the
860 intrinsic fluorescence of NG. Channels are shifted in the insets to facilitate visualization of
861 overlapping ciliary signals. Scale bar 5µm (main panel), 2µm (inset). **D.** The fluorescence
862 intensity of the UbK63 channel in the cilium is represented as violin plots. Asterisks indicate
863 ANOVA significance value. ****, p= <0.0001.

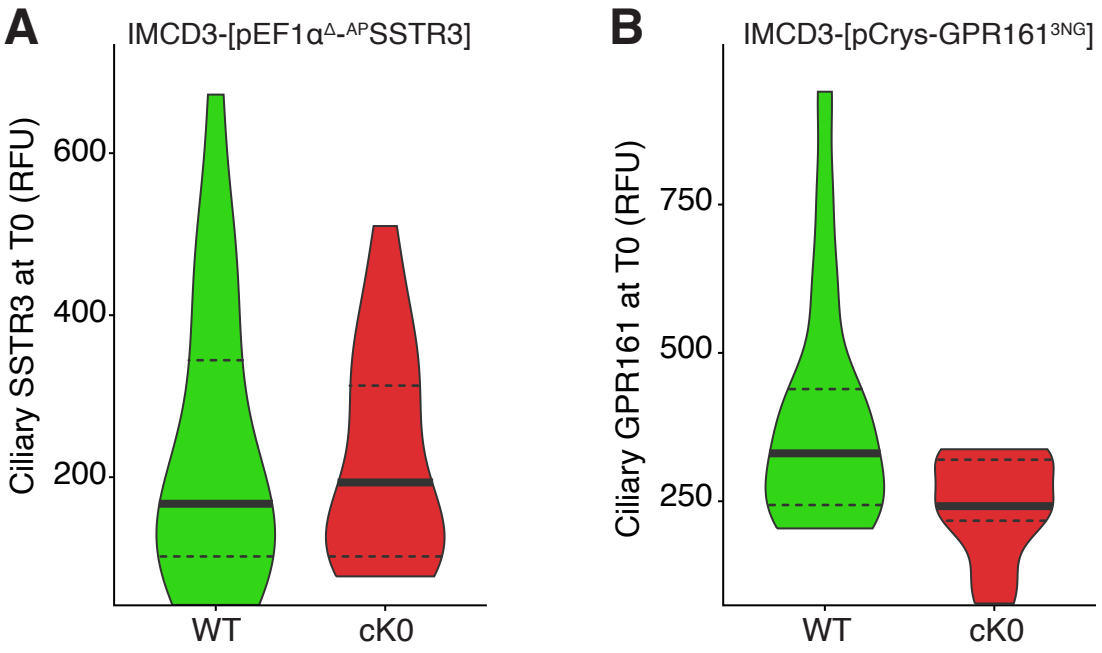


**Supplementary Figure 2**

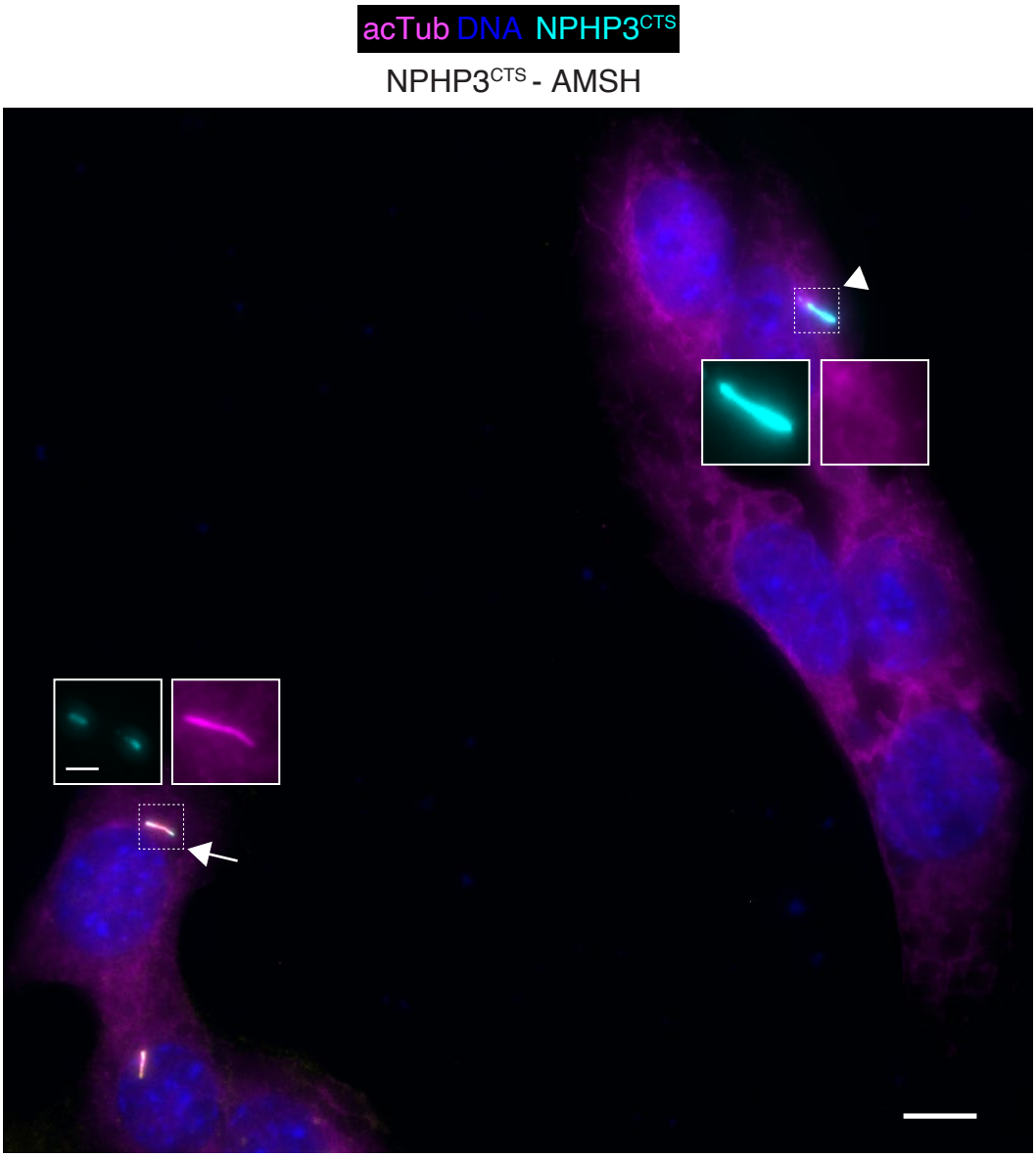


**Supplementary figure 3**

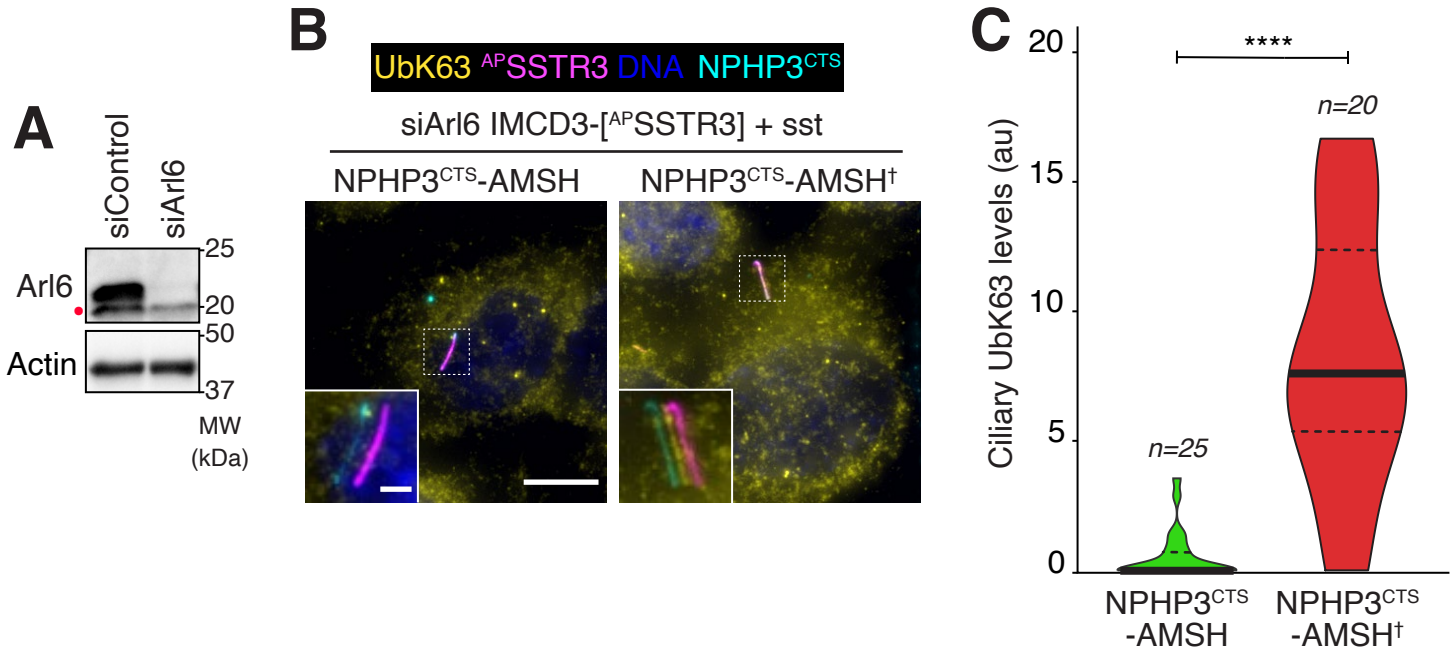


**Supplementary figure 4**

864 **Figure S2. Fluorescence intensities of WT and cK0 GPCR variants at t=0.**

865 **A.** Ciliary $^{AP}$SSTR3 was pulse-labeled by addition of Alexa647-conjugated mSA (mSA647) to the
866 medium for 5-10 min before addition of sst. Violin plots of the ciliary fluorescence intensities for
867 WT and cK0 SSTR3 imaged in the far-red channel at t=0 are shown. **B.** Violin plots of the
868 fluorescence intensities of NG fluorescence corresponding to WT and cK0 GPR161$^{NG}$ at t=0 are
869 shown.

870

871 **Figure S3. Expression levels of ciliary AMSH.**

872 IMCD3-[pEF1α$^{\Delta}$-$^{AP}$SSTR3; pEF1α-BirA•ER] cells were transfected with the plasmid expressing
873 NPHP3$^{CTS}$-AMSH as in Figure 4, before fixation and staining for acetylated tubulin (acTub,
874 magenta) and DNA (blue). The NPHP3$^{CTS}$ fusions were visualized through the intrinsic
875 fluorescence of GFP (cyan) A representative micrograph is shown. A cell expressing modest levels
876 of cilia-AMSH is indicated by an arrow and possesses normal ciliary staining of acetylated
877 tubulin. A cell expressing high levels of cilia-AMSH indicated by an arrowhead displays
878 abnormal ciliary levels of acetylated tubulin. Cells with high ciliary levels of NPHP3$^{CTS}$-AMSH
879 were excluded from the analysis and only cells with modest ciliary levels of NPHP3$^{CTS}$-AMSH
880 were included in the experiment. Scale bar 5μm (main panel), 1μm (inset).

881

882 **Figure S4. Cilia-targeted AMSH removes UbK63 chains from ciliary substrates.**
883 **A.** IMCD3-[pEF1α$^{\Delta}$-$^{AP}$SSTR3; pEF1α-BirA•ER] cells were transfected with control or Arl6
884 siRNAs. Cell lysates were immunoblotted for Arl6 or actin. A non-specific band cross-reacting
885 with the anti-Arl6 antibody is marked with a dot. **B.** IMCD3-[$^{AP}$SSTR3; BirA•ER] cells were
886 transfected with siRNA targeting Arl6 and plasmids expressing NPHP3$^{CTS}$-AMSH or
887 NPHP3$^{CTS}$- AMSH$^{\dagger}$. Surface-exposed $^{AP}$SSTR3 was pulse-labeled with mSA647 for 5-10 min
888 and cells were then treated with sst for 2h before fixation and staining for K63-linked ubiquitin
889 chains (UbK63, yellow). The NPHP3$^{CTS}$-AMSH fusions were visualized through the intrinsic
890 fluorescence of GFP (cyan), $^{AP}$SSTR3 was visualized via mSA647 (magenta) and DNA is blue.

Channels are shifted in the insets to facilitate visualization of overlapping ciliary signals. Scale bar 5μm (main panel), 2μm (inset). **C.** The fluorescence intensities of the UbK63 signal inside cilia are represented as violin plots. Asterisks indicate Mann Whitney test significance value. ****, p= <0.0001.

898 **MATERIALS AND METHODS**

899 **Cell culture**

900 The mouse IMCD3 cell lines used in the study were generated from a parental IMCD3-FlpIn
901 cell line (gift from P.K. Jackson, Stanford University, Stanford, CA). IMCD3-FlpIn cells were
902 cultured in DMEM/F12 (11330-057; Gibco) supplemented with 10% FBS (100-106; Gemini
903 Bio-products), 100 U/ml penicillin-streptomycin (400-109; Gemini Bio-products), and 2 mM L-
904 glutamine (400-106; Gemini Bio-products). The RPE1-hTERT cell line (ATCC CRL-4000) was
905 cultured in DMEM/F12 supplemented with 10% FBS, 100 U/ml penicillin-streptomycin, 2 mM
906 L-glutamine and 0.26% sodium bicarbonate (25080; Gibco).

907 Ciliation was induced by serum starvation in media containing 0.2% FBS for 16 to 24 h.

908

909 **Plasmid construction and Generation of stable cell lines**

910 Stable isogenic IMCD3 cell lines were generated using the Flp-In system (ThermoFisher
911 Scientific). Low-expression promoters and additional expression cassettes were introduced into
912 pEF5/FRT plasmid as described (Nager et al., 2017; Ye et al., 2018). To reduce expression
913 levels, the EF1α promoter was attenuated by mutating the TATA-box (pEF1α$^{\Delta}$) or replaced with
914 a minimal chicken lens δ-crystallin promoter (pCrys).

915 Coding sequences were amplified from plasmids encoding mouse GPR161 (BC028163;
916 Mammalian Gene Collection [MGC]; GE Healthcare), mouse SSTR3 (gift from Kirk Mykytyn,
917 Ohio State University, Columbus, OH), and human BBS5 (gifts from V. Sheffield, University of
918 Iowa, Iowa City, IA), BirA-ER (gift from Alice Ting). β-arrestin 2 (a gift from Mark Scott) was
919 stably expressed from a pCMV-based plasmid (pEGFP-N). SSTR3 and SMO expression were
920 driven by pEF1α$^{\Delta}$, GPR161 expression by pCrys, and BBS5 expression by pEF1α. Coding
921 sequences were fused to GFP, mNeonGreen (NG, (Shaner et al., 2013), or an acceptor peptide
922 for the biotin ligase BirA (AP) (Howarth and Ting, 2008). Multiple rounds of site-directed
923 mutagenesis were performed to generate SSTR3-cK0, a variant with all the cytoplasm-facing

924 lysine residues (K233, K330, K356, K407, and K421) mutated to arginine. GPR161-cK0, a
925 variant with 18 cytoplasm-exposed lysine residues (K83, K84, K93, K167, K247, K250, K269,
926 K296, K358, K362, K455, K469, K473, K481, K486, K497, K504, and K548) mutated to
927 arginine, was gene synthesized (GenScript). Cilia-AMSH was generated by fusing the catalytic
928 domain of mouse AMSH (gift from David Komander; Addgene plasmid #66712; (Michel et al.,
929 2015) with NPHP3(1-200) and GFP to create NPHP3[1-200]-GFP-AMSH[243-424]. A
930 catalytically dead version of AMSH was generated by mutating the water-activating Glu280
931 residue to Ala (Sato et al., 2008; Huang et al., 2013). pRK5-HA-Ubiquitin WT, K0 (all seven
932 acceptor lysine residues – K6, K11, K27, K29, K33, K48, and K63, are mutated to arginine) ,
933 and K63 only (all lysines except K63 mutated to arginines)(gift from Ted Dawson; Addgene
934 plasmid numbers – 17608, 17603, and 17606 respectively).

935 CRISPR-edited *Arl6*$^{-/-}$ and *Arl6*$^{-/-}$/*Arrb2*$^{-/-}$ cell lines were described previously (Liew et al., 2014;
936 Nager et al., 2017). The genotypes are *Arl6*, NM_001347244.1:c.- 10_25del; c.3_6del; and *Arrb2*,
937 NM_001271358.1:c.1 12del;c112_113del.

938

939 **Transfection**

940 For generation of all stable cell lines except for the ones expressing β-arrestin 2$^{GFP}$, FRT-based
941 plasmids were reverse transfected using XtremeGene9 (Roche) into IMCD3 Flp-In cells along
942 with a plasmid encoding the Flp recombinase (pOG44) and stable transformants were selected by
943 blasticidin resistance (4 µg/ml). The transfection mixture was then added to the cells. pEGFP-N•
944 β-arrestin 2-GFP was transfected into IMCD3 cells using Lipofectamine 2000, and clones were
945 selected using neomycin resistance.

946

947 **Antibodies and drug treatments**

948 The following monoclonal antibodies were used for immunofluorescence: anti-acetylated tubulin
949 (mouse; clone 6-11B-1; Sigma-Aldrich; 1:500), anti-ubiquitin clone FK2 was used in all

950 experiments except where indicated (mouse; D058-3; Medical and Biological Laboratories;
951 1:500), anti-ubiquitin FK1 in **Fig. S1A-B** (mouse; D071-3; Medical and Biological Laboratories;
952 1:500), anti-ubiquitin K48 linkage (rabbit; clone Apu2; 05-1307; Millipore-Genentech; 1:500),
953 anti-ubiquitin K63 linkage (human; clone Apu3; a gift from Genentech; 1:500). The following
954 monoclonal antibodies were used for immunoblotting: anti-ubiquitin (mouse; clone P4D1; 3936;
955 Cell Signaling; 1:1000), anti-α tubulin (mouse; clone DM1A; MS-581-P1ABX; Thermo
956 Scientific;1:1000), anti-HA (mouse; clone 16B12; 901501; Biolegend;1:500), streptavidin-HRP
957 (Pierce-21140;Thermo Scientific; 1:10000). The following polyclonal antibodies were used for
958 immunofluorescence: anti-GPR161 (rabbit; 13398-1-AP; Proteintech; 1:100), anti-Smoothened
959 (rabbit; a gift from Kathryn Anderson, Memorial Sloan Kettering Cancer Center, New York,
960 NY; 1:500), anti-cone-arrestin (rabbit; AB15282; Millipore; 1:500). Biotinylated SSTR3 and
961 GPR161 were detected using Alexa Fluor 647–labeled monovalent streptavidin (mSA647) (Ye et
962 al., 2018). The following reagents were used at the indicated concentrations: 200 nM SAG and
963 10 μM somatostatin 14. Somatostatin 14 stocks were made in DMEM/F12 media, HEPES, no
964 phenol red (11039-021, GIBCO). SAG was dissolved in DMSO (276855, Sigma-Aldrich).

965

966 **Imaging and microscopy**

967 Cells were imaged either on a DeltaVision system (Applied Precision) equipped with a PlanApo
968 60x/1.40 objective lens (Olympus), CoolSNAP HQ2 camera (Photometrics), and solid-state
969 illumination module (InsightSSI), or on a confocal LSM 700 (Zeiss) microscope equipped with
970 40x Plan-Apochromat 1.3 DIC oil objective. Z stacks were acquired at 0.5 μm interval (LSM
971 700, Figs. 1, 3, 7, and S1) or 0.2 μm interval (DeltaVision, Figs. 4, 6, S3, and S4).

972 For fixed imaging, 60,000 cells were seeded on acid-washed coverglass (12 mm #1.5; 12-545-81;
973 Thermo Fisher Scientific). Cells were grown for 24 h and then starved for 16-24 h in 0.2% FBS
974 media before experimental treatment. After treatment, cells were fixed with 4%
975 paraformaldehyde in PBS for 15 min at 37°C and extracted in -20°C methanol for 5 min. Cells
976 were then permeabilized in IF buffer (PBS supplemented with 0.1% Triton X-100, 5% normal

977 donkey serum (017-000-121; Jackson ImmunoResearch Laboratories), and 3% bovine serum
978 albumin (BP1605-100; Thermo Fisher Scientific)), incubated at room temperature for 1h with
979 primary antibodies diluted in IF buffer, washed three times in IF buffer, incubated with
980 secondary antibodies (Jackson ImmunoResearch Laboratories) diluted in IF buffer for 30 min,
981 and washed three times with IF buffer. DNA was stained with Hoechst 33258 (H1398; Molecular
982 Probes), cells were washed twice more with PBS, and coverglass mounted on slides using
983 fluoromount-G (17984-25; Electron Microscopy Sciences).

984 For live-cell imaging, 300,000 cells were seeded on acid-washed 25mm cover glass (Electron
985 Microscopy Sciences). After 24 h of growth, cells were serum starved for 16 h and transferred to
986 the DeltaVision stage for imaging at 37°C within an environmental chamber that encloses the
987 microscope and the stage. Cells were imaged in DMEM/F12 media, HEPES, no phenol red
988 (11039-021, GIBCO). To measure SSTR3 exit, cells expressing $^{AP}$SSTR3 were first washed three
989 times with PBS and then pulse-labeled with 2µg/ml mSA647 for 5 min at 37°C. Cells were then
990 imaged after addition of sst (for SSTR3) or SAG (for GPR161) for 2 h with an acquisition every
991 10 min. Each acquisition consisted of a 3-plane Z-stack with each plane separated by 0.5 µm.
992 Transmittance was set to 5% and exposure time to 500 ms.

993 WT or *Bbs4*$^{-/-}$ mice (Mykytyn et al., 2004) eyes were enucleated at P21. Whole eyes were fixed in
994 4% paraformaldehyde/PBS overnight at 4°C and then washed three times with PBS. The eyes
995 were infiltrated in 30% sucrose/PBS at 4 °C overnight. Eyes were placed in OCT compound
996 embedding medium (4583; Tissue-Tek), frozen on dry ice, and stored at −80 °C. 14 µm sections
997 were cut on a cryostat (CM 1850; Leica). Sections were processed for immunofluorescence as
998 follows. Sections were blocked in blocking solution (50 mM Tris pH7.4, 100 mM NaCl, 0.1%
999 Triton-X 100, 3% normal donkey serum, and 0.1% BSA) for 1 h at room temperature, then
1000 incubated with primary antibodies overnight at 4°C, followed by three washes in wash solution
1001 (50 mM Tris pH7.4, 100 mM NaCl, and 0.1% TX100). After rinsing in wash solution, sections
1002 were incubated with secondary antibodies for 1 h at room temperature. DNA was counterstained
1003 using Hoechst 33258 dye, sections washed twice more with PBS, and mounted on slides using
1004 Fluoromount-G. Sections were imaged on Confocal LSM 700 (Zeiss ) microscope.

1005

1006 **Image analysis**

1007 Files were imported from the Deltavision or LSM700 workstations into ImageJ/ Fiji (National
1008 Institutes of Health) for analysis. For the quantification of ciliary ubiquitin signal in fixed cells,
1009 maximum intensity projections were used. The ciliary ubiquitin intensity was measured using the
1010 following equation:

1011 $F_{Ub\text{-}cilia} = F_{Ub\text{-}cilia_measured} - F_{background}$

1012 $F_{Ub\text{-}cilia_measured}$ is the total ciliary ubiquitin fluorescence detected, $F_{background}$ is the background
1013 ubiquitin fluorescence measured in the adjacent area. For all measurements, the fluorescence
1014 integrated density was used. $F_{Ub\text{-}cilia}$ were plotted as violin plots using the PlotsOfData web tool
1015 (https://huygens.science.uva.nl/PlotsOfData/). Each violin represents the distribution of data,
1016 which includes all the data points. Median and interquartile range is marked by solid and dotted
1017 lines, respectively. No gamma adjustment was applied during figure preparation; all the
1018 representative micrographs for respective panels are displayed within the same dynamic range.
1019 For some representative micrographs, the most in-focus plane was used rather than the
1020 maximum intensity projection (Fig.3, and Fig. 6, panel A and C).

1021 To measure SSTR3 exit, the integrated density of Alexa Fluor 647 fluorescence in the maximum
1022 intensity projection was measured for each time point. The cilia-adjacent fluorescence was
1023 subtracted as the background, and a mathematical photobleaching correction was applied:

1024 $F_{cilia} = (F_{mSA647_measured}/F_{mSA647_1}) + ((1 - e^{-\lambda}) * (n - 1))$, where $\lambda$ is the photobleaching decay
1025 constant, n is the number of images taken, $F_{mSA647_measured}$ is the integrated mSA647 fluorescence
1026 measured for image n, $F_{mSA657_1}$ is the measurement for the first time point, and $F_{cilia}$ is the
1027 reported fluorescence. In this equation, $F_{cilia}$ is reported in relative fluorescence units (RFUs).
1028 $^{AP}GPR161^{3NG}$ exit was followed similarly with the difference that NG fluorescence intensity was
1029 measured. For SSTR3 as well as GPR161, photobleaching corrected data ($F_{cilia}$) for each
1030 condition were linearly fitted ($F_{cilia} = m * time + c$) and plotted in Excel.

1031 Endocytosed SSTR3 foci were revealed by contrast enhancement and counted with the ImageJ
1032 particle analysis tool.

1033 ***Chlamydomonas* culture, isolation of flagella and immunofluorescence**

1034 *Chlamydomonas* WT- g1 (nit1, agg1, mt+) [gift from George B. Witman, University of
1035 Massachusetts Medical School, Worcester, Massachusetts]and *Bbs4*- CC-4377 ptx5-1/bbs4-1::
1036 NIT1 agg1 mt+ (Chlamydomonas Resource Center) strains were cultured asynchronously under
1037 light in TAP media (Gorman and Levine, 1965) for 72 h. Flagellar fractions were prepared from
1038 two liters of cultures of WT or *Bbs4* cells as described (Craige et al., 2013). Briefly, cells were
1039 harvested by centrifugation for 5 min at 2,000 rpm (1,100 x *g*) at room temperature. Cells were
1040 resuspended in 10 mM HEPES, pH 7.4 and centrifuged for 5 min at 2,000 rpm (1,100 x *g*). Next,
1041 the cell pellet was gently resuspended in ice-cold HMDS (10 mM HEPES, pH 7.4, 5 mM
1042 $MgSO_4$, 1 mM DTT, and 4% (w/v) sucrose). Deflagellattion was achieved by addition of 5 mM
1043 dibucaine to each tube of cells and by pipetting up and down ~10 times using a 10-ml plastic
1044 serological pipette. The suspension was spun for 5 min at 1,800 x *g* at 4°C. The supernatant
1045 containing flagella was underlaid with 9 ml ice-cold HMDS-25% sucrose (10 mM HEPES, pH
1046 7.4, 5 mM $MgSO_4$,1 mM DTT, and 25% (w/v) sucrose), followed by a centrifugation step for 10
1047 min at 2,800 rpm (2,400 x *g*), 4°C. The supernatant above the sucrose interface was collected
1048 using a 25-ml serological pipette and flagella were pelleted by centrifugation for 20 min at 30,000
1049 x *g* (16,000 rpm), 4°C. The flagellar pellet was resuspended in 100 µl HMDS buffer. Protein
1050 concentrations were measured by Bradford and 25 ug were resolved by SDS-PAGE for
1051 immunoblotting.

1052 *Chlamydomonas* immunofluorescence was performed as follows. Cells were fixed with 4 %
1053 paraformaldehyde in MT buffer* (30 mM HEPES, pH7, 5 mM EGTA, 5 mM MgSO4, and
1054 25mM KCl) for 20 minutes in suspension. The cells were centrifuged at 1000 rpm for 5 minutes,
1055 resuspended in 100 µl of fixative and transferred onto slides coated with 1 mg/ml poly-L-lysine.
1056 After 5 minutes, the unadhered cells were washed off by rinsing with PBS. Cells were
1057 permeabilized in 0.5% Triton-X 100 for 20 minutes followed by blocking for 1 h in blocking
1058 buffer (3% fish skin gelatin, 1% BSA, 0.1% Tween20 in PBS) at room temperature. Cells were

1059 incubated at 4°C overnight with primary antibodies diluted in blocking buffer, washed five times
1060 in PBS and incubated with secondary antibodies for 2 h at room temperature. After five washes
1061 in PBS, coverglasses were mounting on slides using Fluoromount-G. Cells were imaged on the
1062 LSM700 confocal microscope.

1063

1064 **Biochemical analysis of SSTR3 ubiquitination**

1065 IMCD3 cells stably expressing pEF1α$^{\Delta\text{-AP}}$SSTR3$^{NG}$ and BirA-ER were transiently transfected
1066 with HA-tagged ubiquitin plasmids. Cells were reverse transfected using XtremeGene9 and
1067 plated into 15 cm plates. Cells were moved to medium containing 0.2% serum and
1068 supplemented with 10 µM biotin 24 h after transfection to promote ciliation and maximize
1069 biotinylation of SSTR3. 18h after the medium change, sst was added for 0, 10 or 20 min. The
1070 assay was stopped by washing cells twice with ice-cold 1xPBS and scraping cells off on ice into
1071 1ml of ice-cold RIPA buffer (50 mM Tris/HCl pH 8, 150 mM NaCl, 1% Nonidet P-40, 0.5%
1072 sodium deoxycholate, 0.1% SDS, 100 mM iodoacetamide, 10mM EDTA) supplemented with
1073 protease inhibitors (1 mM AEBSF, 0.8 mM Aprotinin, 15 mM E-64, 10 mg/mL Bestatin, 10
1074 mg/mL Pepstatin A and 10 mg/mL Leupeptin). After gently rocking at 4°C for 5 minutes,
1075 lysates were clarified by spinning in a tabletop Eppendorf centrifuge at 15,000 rpm and 4°C for
1076 20 minutes. Each clarified lysate was incubated with 50µl of streptavidin Sepharose beads (GE
1077 Healthcare) for 1 h at 4°C to capture biotinylated SSTR3. Beads were washed four times with
1078 500µl of RIPA buffer and bound proteins were eluted by heating the beads in 1X LDS sample
1079 loading buffer containing 2 mM biotin at 70°C for 10 minutes. After SDS-PAGE and transfer,
1080 PVDF membranes were probed with anti-HA antibody and streptavidin-HRP.

1081 Signals were acquired with a ChemiDoc imager (Bio-Rad) and analyzed with ImageLab 6.0.1
1082 (Bio-Rad). The integrated densities of the SSTR3 bands in the streptavidin-HRP blot were
1083 normalized to the integrated densities of the endogenous biotinylated proteins to correct for
1084 variations in the recovery of biotinylated proteins on streptavidin Sepharose. The resulting value
1085 is SSTR3$_{bio}$. Second, the integrated densities of ubiquitinated SSTR3 were collected by

1086 measuring the area from 100 kDa to the top of the gel on the HA blot. The values were
1087 background-corrected by subtracting the value of the equivalent area in the IMCD3 control lane.
1088 The resulting value is Ub-SSTR3$_{raw}$. The relative amount of SSTR3 that is ubiquitinated, Ub-
1089 SSTR3$_{frac}$ = Ub-SSTR3$_{raw}$/SSTR3$_{bio}$ was plotted on the graphs using PlotsOfData (Postma and
1090 Goedhart, 2019).

1091